*Annual Review of Fluid Mechanics*

# The Role of Canopy Turbulence in Wildland Fire Behavior

Tirtha Banerjee

Department of Civil and Environmental Engineering; Department of Earth System Science, University of California, Irvine, California, USA; email: tirthab@uci.edu



Annu. Rev. Fluid Mech. 2026. 58:473–502

The *Annual Review of Fluid Mechanics* is online at fluid.annualreviews.org

https://doi.org/10.1146/annurev-fluid-112723-062216



## Keywords

buoyant plumes, Byram convective number, canopy heterogeneity, canopy turbulence, counterrotational vortices, crown fire, fire–vegetation–atmosphere interaction, sweep–ejection, tower–troughs, wildland fire entrainment

## Abstract

Characterizing the physical and dynamic meteorology of wildland fires has obvious socioeconomic importance and is necessary to develop not only fire-fighting but also mitigation strategies such as prescribed burns and effective fuel management practices such as forest thinning. However, despite significant progress over a century, there are shortcomings in our understanding of the physical processes governing wildland fire behavior. Although some research progress has been made in understanding how fires spread on grasslands, several aspects of fire behavior within the forest canopy environment are still not well-understood. This review is an attempt to organize the fluid mechanics of the mass, momentum, and energy transfer during wildland fire events through the lens of vegetation canopy turbulence. The structure, organization, and progress of the flame front and the buoyant plume through the canopy are shown to be intricately related to the coherent structures associated with fire–vegetation–atmosphere interaction, and potential future research directions are identified.

# 1. INTRODUCTION

## 1.1. Motivation and Background

Wildland fire behavior differs quite significantly in grassland and with shrub-type fuels as opposed to in vegetated environments. In grassland environments, the fuel depth is much shorter, and the flames interact with the open atmospheric boundary layer above the fire. In a vegetated environment, the fire occurs in the canopy sublayer (Poggi et al. 2004), as shown in **Figure 1**.

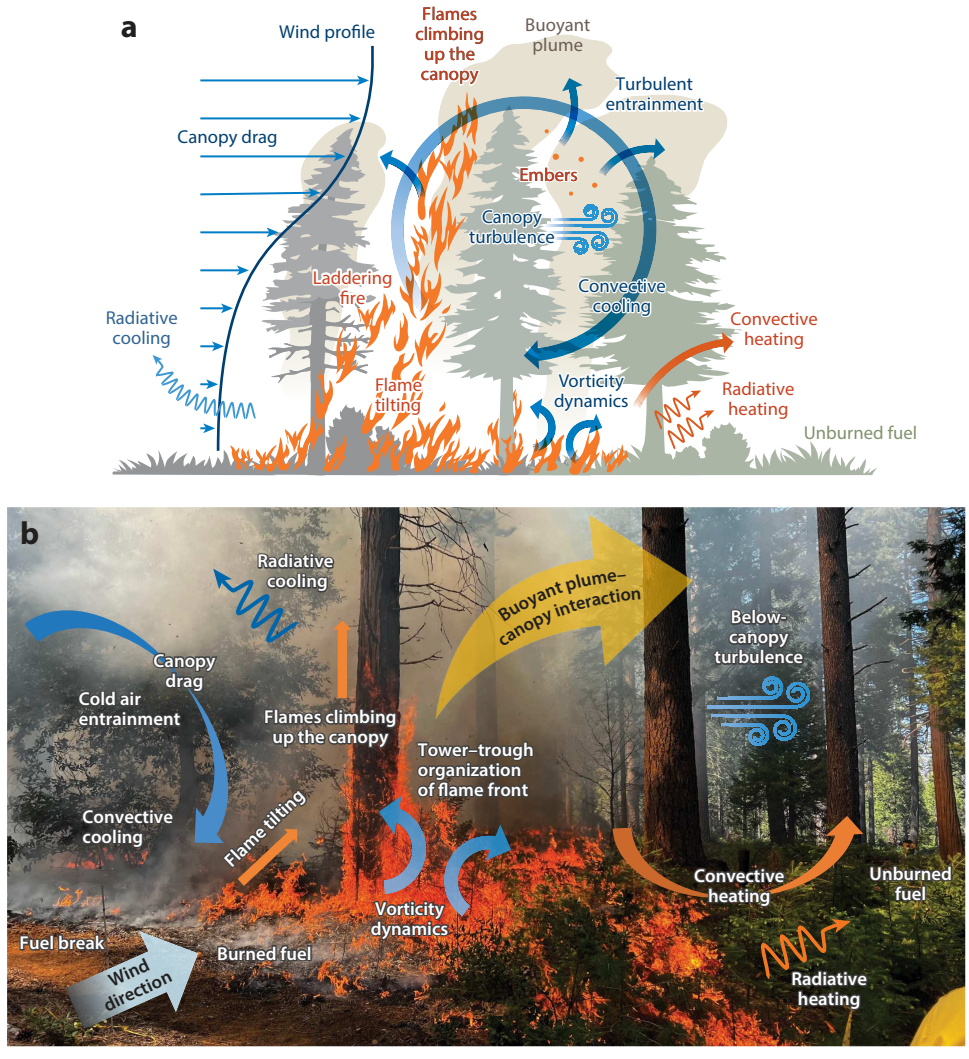


**Figure 1**

Key features of vegetation canopy turbulence associated with wildland fire–vegetation–atmosphere interaction, shown using (*a*) a conceptual schematic and mapped onto (*b*) a photograph of a prescribed fire in the Blodgett Forest Research Station, California. The figure shows flame tilting due to ambient wind, laddering behavior of flames, fire progression by convective and radiative heating of downwind fuels, cold air entrainment and associated convective cooling, radiative cooling of burning fuels, tower–trough structures of the flame front, and buoyant plume dynamics interacting with subcanopy turbulence, all of which are discussed in the subsequent sections.

Below-canopy turbulence is characterized as a roughness sublayer flow (Harman & Finnigan 2007) and is more representative of a mixing layer, rather than a canonical boundary layer. The implication is that canopy-induced turbulent eddies interact with the fire and the fire–atmosphere interaction is modulated by the fundamental nature of canopy turbulence (Heilman et al. 2015, 2021; Banerjee 2020; Banerjee et al. 2020a; Bebieva et al. 2020; Heilman 2021, 2023).

The forest canopy acts as an extended sink of momentum by imparting drag for the air above, thereby imposing a range of length and velocity scales. Moreover, the presence of shear-induced instabilities at the canopy–atmosphere interface results in intermittent coherent structures that penetrate the subcanopy airspace and aid in canopy–atmosphere interaction. The physics of turbulent flow in vegetated canopies itself is an active area of research to date (Raupach & Thom 1981, Finnigan 2000, Belcher et al. 2012, Nepf 2012, Patton & Finnigan 2012, Brunet 2020, Finnigan 2020). Standard atmospheric boundary layer formulations are inadequate in explaining the canopy–atmosphere exchange of mass, momentum, and energy. This is further complicated by the presence of the fire, which generates additional shear and buoyancy-induced motions. In addition, under certain circumstances, surface fires occurring in a vegetated environment can climb up ladder fuels (**Figure 1**) and damage the canopy (Van Wagner 1977, Banerjee 2020, Banerjee et al. 2020a). Moreover, if the conditions are favorable, the fire can spread horizontally from canopy to canopy, becoming a much higher-intensity crown fire (Van Wagner 1977).

Understanding the fluid mechanics of how wildland fires behave and spread is therefore of utmost importance for a large and diverse clientele, spanning ecology, climatology, atmospheric science, engineering, hydrology, and more. Each of these disciplines is interested in the behaviors or implications of wildland fire behavior on a different scale or in a different context, all of which require an understanding of different aspects of the fluid mechanics of fire–vegetation–atmosphere interaction (see the sidebar titled Scales and Processes: Canopy Turbulence and Fire–Vegetation Interaction).

For example, the ventilation of smoke from wildland fires and therefore the air quality impact is strongly dependent on the turbulent buoyant plume dynamics and its interaction with the forest structure (Heilman 2023). Another example is the spotting behavior of firebrands, which can travel long distances and create spot fires and damage structures during wildfires. The spotting distance is strongly dependent on the ejection characteristics of these particles, which are also a function of the near-surface atmospheric turbulence (Chung & Koseff 2023, Chung et al. 2024, Petersen & Banerjee 2024). Additionally, a detailed understanding of the sensitivity of wildland fire spread to changes in the forest structure (Marcozzi et al. 2025) is necessary to develop both firefighting (Legendre 2024) and mitigation strategies such as prescribed burns and effective fuel management practices (Hiers et al. 2020, Bonner et al. 2024, Li et al. 2025). Fuel treatment techniques such as forest thinning could also have unintended consequences, such as higher fire intensity and rate of spread (ROS) because of a drier and windier subcanopy marked by higher levels of turbulence (Banerjee 2020, Banerjee et al. 2020a, Heilman 2021). To assess the effectiveness of such management efforts, as well as the previous applications, it is crucial to understand wildland fire behavior inside the canopy environment (**Figure 1**).

**Coherent structure:** large, organized pattern in turbulent flow that dominates energy transport

**Spotting:** small fires created by firebrands or embers away from the main fire front

**Firebrand:** particles or debris originating from burning fuels

**Prescribed burn:** small-scale intentional fire designed to reduce fuel load and attain other ecological objectives

**Thinning:** mastication of the canopy, lowering fuel availability and canopy drag

**ROS:** rate of spread

## 1.2. State of the Science and Overarching Questions

The role of vegetation canopy in modulating wildland fire spread can be clustered around five thematic topics as found in the literature: (*a*) using experiments and field observations to report statistics of turbulent quantities in the presence of vegetation canopies (Beer 1991; Kenney et al. 2008; Mueller et al. 2014, 2021b; Linn et al. 2013; Heilman et al. 2015; Kiefer et al. 2015; Sullivan 2017; Bebieva et al. 2020, 2021; Clark et al. 2020; Mallia et al. 2020; Zhang & Lamorlette 2020; Heilman 2021; Katurji et al. 2021, 2022; Valencia et al. 2023), (*b*) developing

## SCALES AND PROCESSES: CANOPY TURBULENCE AND FIRE–VEGETATION INTERACTION

The turbulent processes associated with wildland fires in forest canopies, by definition, span a narrow range of scales (from subseconds to hours and millimeters to kilometers). It is, however, important to recognize that these small-scale processes are integrators and connectors across a much wider range of scales and processes (**Figure 2*a***). Scales at which vegetation impacts fire regimes and fires impact vegetation span from individual leaves to trees to stands, forests, and entire ecosystems, and from seconds to seasons to climate timescales.

### Connection Between Scales

Long-term ecosystem-scale processes determine the type and amount of fuel, horizontal and vertical fuel distribution, fuel connectivity, fuel dryness, and more through micrometeorological processes. These long-term processes therefore determine the antecedent boundary conditions for a fire to initiate and spread, which are dependent on local and immediate weather conditions, for example, air temperature, wind speed, ambient turbulence levels, and so on. The behavior and impact of the fire in the short timescale determine fuel consumption, crown damage levels, soil health, and seed dispersion. In turn, these processes determine the future state of the landscape, such as the amount of invasive species encroachment, water and light competition among surviving trees, and pattern or patchiness of vegetation. These processes set the boundary condition for future fire spread, thereby closing the loop.

### Studying Different Scales

The smallest scales, that is, the combustion scales, can be studied in laboratories, while the largest-scale processes across ecosystems or years can be studied through satellite remote sensing. The intermediate scales of fire–vegetation–atmosphere interaction are too large to be studied in lab settings and too small to be studied using satellite remote sensing. Therefore, progress in this area has been dependent on a combination of lab and field-scale studies, numerical simulations, and analytical and empirical modeling. To summarize, it is important to recognize the multitude of scales and processes that frame the problem of canopy turbulence in wildland fire behavior. The reader is referred to McKenzie et al. (2011) for a thorough discussion.

**Canopy drag:** aerodynamic resistance caused by foliage; shapes the velocity profile and turbulence characteristics

**Laddering:** upward movement of fires toward the forest canopy

**Crowning:** horizontal tree-to-tree movement of fires across the forest canopy

numerical parameterizations of a forest canopy in wildland fire behavior models primarily using a standard canopy drag parameterization (Linn et al. 2005; Kenney et al. 2008; Mueller et al. 2014, 2021b), (*c*) observation and modeling of fire plume development and spotting above plant canopies (Raupach 1990, Nelson 1993, Mercer & Weber 1994, Sullivan 2007, Albini et al. 2012, Morvan & Frangieh 2018, Arreola Amaya & Clements 2020), (*d*) observations of laddering and crowning behavior (Van Wagner 1977, Graham et al. 2004, Michaletz & Johnson 2006, Morvan 2011, Banerjee 2020, Banerjee et al. 2020a, Moinuddin & Sutherland 2020), and (*e*) using fire behavior models to simulate the sensitivities of canopy-level heterogeneities and other governing fuel parameters such as fuel moisture on wildland fire behavior (Graham et al. 2004; Linn et al. 2005; Peterson et al. 2005; Raymond & Peterson 2005; Harrington & Kathol 2009; Safford et al. 2009; Stephens et al. 2009; Pimont et al. 2011; Hoffman et al. 2015; Kiefer et al. 2016, 2018; Hoff et al. 2019; Accary et al. 2020; Atchley et al. 2021; Mueller et al. 2021a).

This article is aimed at organizing the vast and seemingly disparate literature of wildland fires systematically under the umbrella of the canopy turbulence literature. With this goal, the overarching questions can be framed as follows: How do the turbulent coherent structures imposed by the canopy influence the convective and radiative regimes that regulate fire spread, and what differentiates coupled fire–canopy–atmosphere interaction from standard canopy turbulence? This

framework also alters the current fuel-centric perspective in the wildland fire literature (McKenzie et al. 2011, Loudermilk et al. 2022), in which the vegetation appears as mere fuel to be consumed by the flames, to a different paradigm, in which the canopy itself actively modulates the wind and the fire through interactions spanning multiple scales (**Figure 2*a***).

## 1.3. Historical Developments

Some of the first systematic studies that can be found under the theme of the role of canopy turbulence in wildland fire spread are operational in nature, with an emphasis on finding simple relationships between environmental factors such as wind, slope, temperature, and humidity and the ROS of wildland fires (**Figure 2*b–g***). Show (1919) is one of the earliest examples of such studies based on a series of experimental fires conducted between 1915 and 1917 in the Feather River Experimental Station, a US Forest Service facility in the Sierras in Northern California. The fire ROS was found to vary as the square of the wind velocity, using a simple data-fitting exercise of empirical observations. It was also noted that the release of a large amount of heat in a short period creates a convective current of air, which increases the wind velocity and therefore the ROS—"a fire creates its own draft" (Show 1919, p. 975).

The next set of developments can be found in Canada, since extreme boreal fires were deemed a leading cause of forest destruction. A technical report from the Canadian Forest Service (Wright 1932) published results in line with Show (1919), finding that the velocity squared law was applicable for active experimental fires conducted at the Petawawa Forest Experimental Station in 1929. In addition, they investigated the role of other factors such as moisture, air temperature, relative humidity, duff temperature, solar radiation, and rate of evaporation in creating favorable conditions for fire spread; these can be summarized as micrometeorological features in the subcanopy environment. Wright (1932) also highlighted the need to estimate below-canopy wind speed since the measurements were made above the canopy, one of the most important problems in the general research area of forest canopy turbulence (Finnigan 2000).

The next set of systematic studies linking canopy processes and fire behavior can be found in the United States, notably by Curry & Fons (1940). One significant contribution from this work is the attempt to correlate wind velocity within the forest stand and wind measurements in the open. The authors reported experimental data for the vertical wind velocity profile in open grassland and a dense coniferous forest (**Figure 2*d***). These profiles are easily recognized by researchers working in the realm of atmospheric boundary layers—the grassland velocity profile is logarithmic in nature, and the velocity profile in the forest canopy is logarithmic above the canopy and attenuates exponentially within the canopy. It is notable that these results were published 34 years before the study by Shaw et al. (1974), which reported velocity profile statistics data over a corn canopy showing similar features and is usually recognized as the earliest systematic study of such velocity statistics (Kaimal & Finnigan 1994) in the atmospheric boundary layer literature.

Another notable advancement made by Curry & Fons (1940) was the identification of fuel particle variables (such as the surface area per unit volume, which differentiates between fine and coarse fuels) and fuel bed variables (such as the volume of voids per fuel surface area). This is a recognition that individual fuel element properties are important for combustion, but for the spread of fires within a fuel complex, it is the collective property of the fuel structure (extrapolated as a canopy-level emergent property) that is important, since the available airspace between voids influences oxygen supply and distribution of radiative energy, which would impact the rate at which the exposed fuel surface would absorb heat and ignite progressively, allowing the fire to spread. This would set the stage for future modeling by Rothermel (1972) and Albini (1985).

Subsequently, Fons (1946) presented an energetics-based model to explain the rate of fire spread through rod-like fuel elements, using experiments conducted in a wind tunnel using

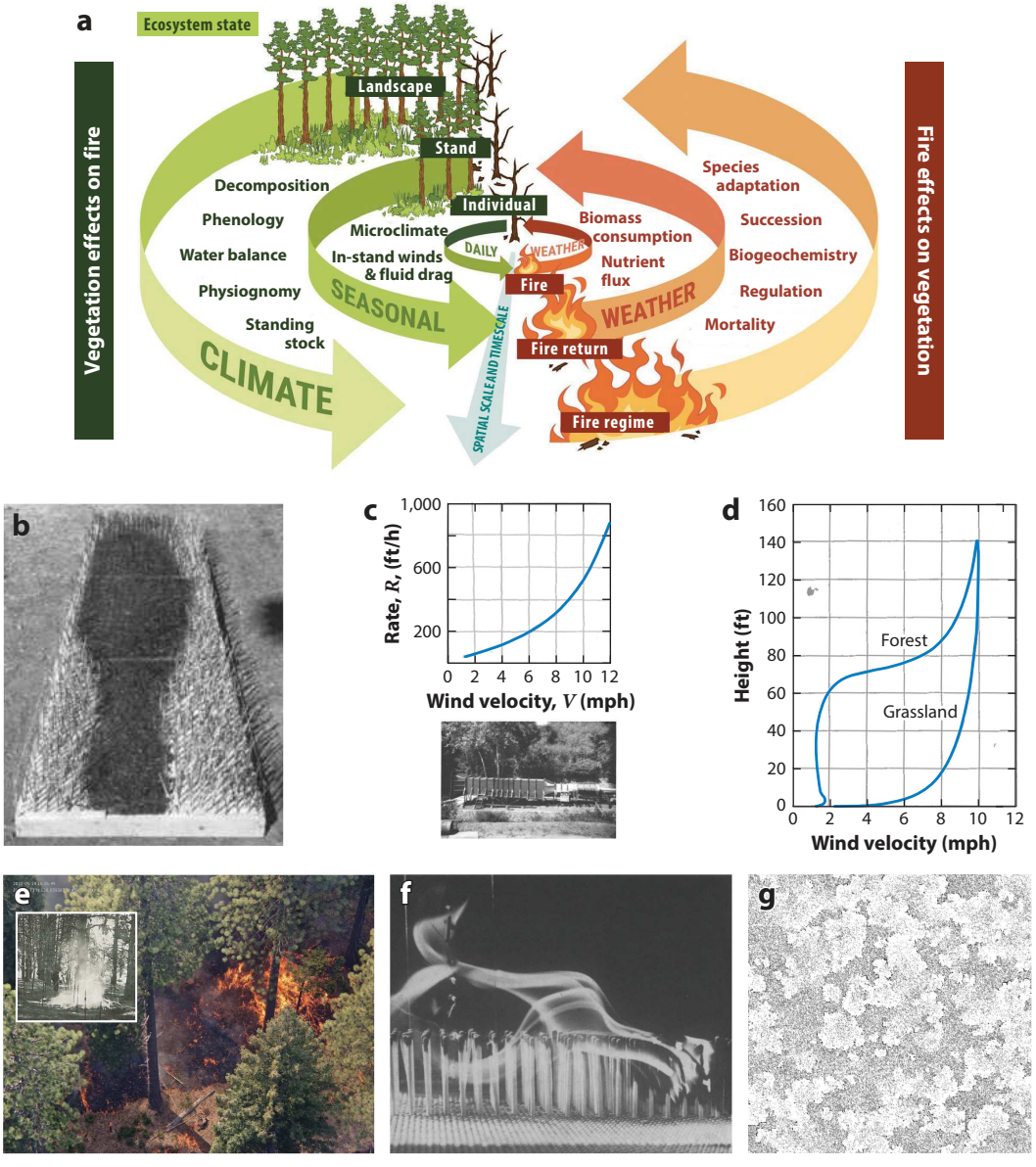


**Figure 2**

(*a*) Two-way interaction of wildland fires and vegetation across a wide range of spatial and temporal scales. Panel adapted from Loudermilk et al. (2022) (CC BY 4.0). (*b*) Typical burned area from the wind tunnel experiments by Fons (1946). (*c*) Empirical relation between rate of spread and wind speed reported by Fons (1946) (*top*) and the wind tunnel used by Fons (1946) (*bottom*). Panels *b* and *c* adapted from Fons (1946) (public domain). (*d*) Typical vertical mean velocity profile over a forest and a grassland. Panel adapted from Curry & Fons (1940) (public domain). (*e*) A modern fire behavior experiment imaged by a uncrewed aerial vehicle conducted by the author in Northern California with similar experiments conducted by Curry & Fons (1940) shown in the inset. (*f*) Matchstick-bed experiment by Beer (1991). Air flow is from right to left. Panel adapted with permission from Beer (1991). (*g*) Snapshot of an agent-based simulation following Clar et al. (1997) and Charbonneau (2017), where every dot represents a tree and the landscape is depicted after several cycles of burning and ecological succession.

ponderosa pine needles as a fuel bed for validation (**Figure 2*b*,*c***). This work considered two mechanisms by which wind velocity can impact ROS. During air flow over the solid canopy fuel elements, a thin film boundary layer develops over the solid surface, and as the wind flow increases, the layer becomes thinner, enhancing the conductance of heat through this layer. Therefore, for forced convection, this film conductance or heat transfer coefficient increases with wind speed from experimental data. Another way the wind would impact the ROS would be the following: With increasing velocity, the flame is tilted more toward the ground, enhancing the contact angle with the fuel and preheating the downstream fuel more efficiently. Therefore, fuel temperature would increase with wind velocity. The collective impact is manifested as an ROS still varying almost as a square of velocity, but now with a more detailed physical interpretation of different heat and mass transfer mechanisms.

By the mid-1980s, the first tenets of canopy turbulence had a solid foundation following the publication of Raupach & Thom (1981). By the early 1990s, wildland fire studies could be found to be connecting with the canopy turbulence literature. Notable examples are publications by Raupach (1990) and Beer (1991), which discussed the implications of canopy-induced sweep–ejection structures on fire spread. Event-wise decomposition of turbulent momentum fluxes revealed that sweeps or downward incursions of high momentum air from the top are most efficient in momentum transfer inside the canopy. Sweeps deliver more of the momentum yet occur very intermittently (Raupach 1990). A small-scale laboratory experiment (**Figure 2*f***) reported by Beer (1991) led to the hypothesis that during a forest fire (when the litter on the forest floor burns but the trees remain standing), the intermittent gusts of strong downward moving air that originate above but penetrate into the canopy (i.e., sweeps) are important for fire spread. This is because advective preheating of the fuel elements downstream of the flame is an important mechanism of fire spread and the sweeping eddies (*a*) help keep a substantial part of the flame embedded with the fuel bed that allows both convective and radiative heating of fuel elements downstream and (*b*) also carry the advective heat flux by their penetrating mechanism themselves. This is revealed in the matchstick-bed fire in **Figure 2*f*** where the smoke illuminates the path of the air flow, clearly showing the advective motions that help carry the heat from the flame on the right to fuel elements deep inside the canopy on the left.

Another parallel development in modeling fires came from the physics community (complex systems science) with the advancement of agent-based modeling, cellular automata, and self-organized criticality (**Figure 2*g***). Notable examples include work by Bak et al. (1990), Beer (1990), Drossel & Schwabl (1992), and Grassberger (1993). Although these agent-based models were not meant for individual fire behavior but for fire behavior in large timescales and spatial scales, recent works have extended this approach toward more practical directions and individual fire events (Ohtsuki & Keyes 1986, Karafyllidis & Thanailakis 1997, Rui et al. 2018).

**Sweep:** downward movement of high-momentum air from aloft

**Ejection:** upward movement of low-momentum air from below

**Resting buoyant plume:** buoyant plume emanating from a nonmoving fire

## 2. SCALING ANALYSIS

In this section, I introduce a generalized dimensional analysis and thereafter discuss relevant scaling variables for resting buoyant plumes and moving fires.

### 2.1. General Dimensional Analysis

As evident in the introductory discussions, a corpus of dimensional relations can be found in the literature that attempt to connect bulk fire behavior properties for both buoyant plumes and moving fires with environmental variables. A dimensional analysis using the Buckingham $\pi$ theorem (Buckingham 1914, Katul et al. 2019) can be conducted as illustrated by Desai et al. (2025b), and

**Table 1 Key variables for dimensional analysis**

| Variable | Symbol | Dimension(s) |
|---|---|---|
| Atmospheric boundary layer height | $\delta$ | $L$ |
| Canopy drag length scale | $L_c = (C_d \mathrm{LAD})^{-1}$ | $L$ |
| Gravity (buoyancy) | $g$ | $LT^{-2}$ |
| Canopy height | $h_c$ | $L$ |
| Effective patch radius (patch area/perimeter) or flame depth | $R_p$ | $L$ |
| Kinematic heat flux difference at surface ($\Delta H_s = H_{patch} - H_{ambient}$) | $\frac{\Delta H_s}{\rho c_p}$ | $KLT^{-1}$ |
| Friction velocity | $u_*$ | $LT^{-1}$ |
| Ambient potential temperature | $T_0$ | $K$ |
| Horizontal length scale for bent plume | $\lambda_{pc}$ | $L$ |

The drag length scale $L_c$ can be defined as a combination of the drag coefficient $C_d$ and the LAD. $K$ denotes the dimension of temperature. Abbreviation: LAD, leaf area density.

it can be demonstrated that the major bulk scaling relations related to wildland fires without and with forest canopies in the literature can be encompassed by this dimensional analysis. The functional forms emerging from this analysis can also be used to guide future experimentation and modeling efforts.

The key variables to be considered are listed in **Table 1**, and the schematic in **Figure 3** depicts the physical context of the variables. With nine variables and three fundamental dimensions, we find $9 - 3 = 6$ dimensionless $\pi$ groups can be formed with three repeating variables $R_p$, $u_*$ and

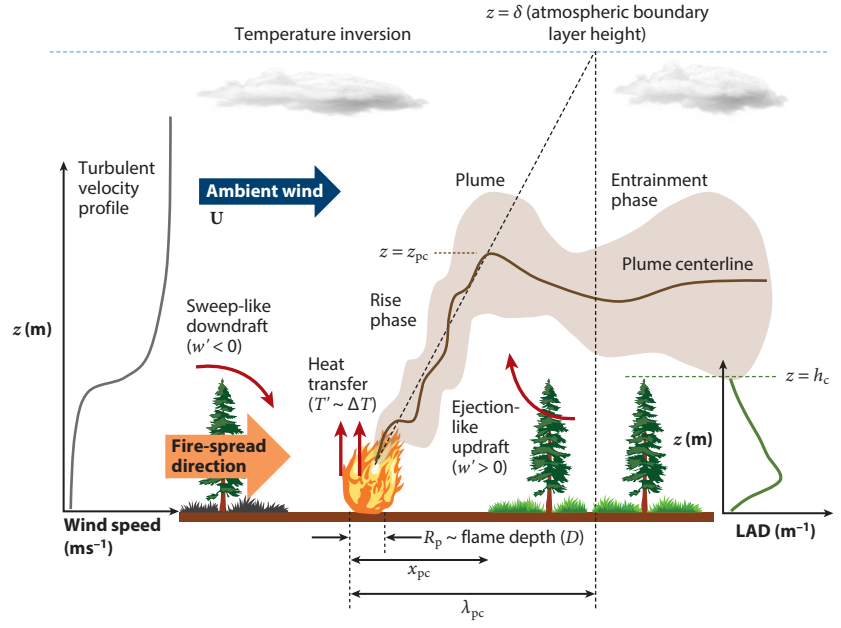


**Figure 3**

Schematic of a fire plume within a forest canopy. Leaf area density (LAD) is depicted with a typical vertical profile.

$T_0$. Therefore, for the scenario with the vegetation canopy, we obtain

$$\frac{\lambda_{pc}}{R_p} = f\left(\frac{\delta}{R_p}, g\frac{R_p}{u_*^2}, \frac{\Delta H_s}{\rho c_p}\frac{1}{T_0 u_*}, \frac{L_c}{R_p}, \frac{b_c}{R_p}\right). \quad 1.$$

For a fire configuration without the canopy (e.g., when the fire is over a grassland), the combination becomes

$$\frac{\lambda_{pc}}{R_p} = f\left(\frac{\delta}{R_p}, g\frac{R_p}{u_*^2}, \frac{\Delta H_s}{\rho c_p}\frac{1}{T_0 u_*}\right). \quad 2.$$

Therefore, the plume slope (relative to the horizontal) can be written as (replacing $\lambda_{pc}$ using Equation 2)

$$\tan(\theta_p) \approx \theta_p = \frac{\delta}{\lambda_{pc}} = \frac{\delta}{R_p}\frac{1}{f}. \quad 3.$$

Note that the dimensionless group $R_p g/u_*^2 \approx Fr^{-2}$ can be described as the inverse square of an equivalent Froude number $Fr \approx \sqrt{u_*^2/R_p g}$. Also note that

$$\frac{\Delta H_s}{\rho c_p}\frac{1}{T_0 u_*} \approx \frac{\overline{w'T'}}{u_*}\frac{1}{T_0}, \quad 4.$$

where $\overline{w'T'}$ is the kinematic vertical sensible heat flux.

If we argue that $T' \approx \Delta T = T - T_0$, the equation above becomes

$$\frac{\Delta H_s}{\rho c_p}\frac{1}{T_0 u_*} \approx \frac{\Delta T}{T_0}\frac{w_*}{u_*}. \quad 5.$$

For further simplification, if we assume that $w_* \sim u_*$ for a fire environment where both shear and buoyancy-driven turbulence are strong, then this dimensionless term can be simply written as $\Delta T/T_0$. It is noted that experimental designs can be performed to investigate the mathematical form of the function $f$ in Equations 1 and 2.

## 2.2. Scaling Analysis for Buoyant Plumes

The interaction of a fire-generated buoyant plume with the forest canopy was studied by Raupach (1990) using similarity analysis. Instead of attempting to express the ROS of the fire front in terms of other environmental variables, Raupach (1990) focused on characterizing the impact of the buoyant plume originating from the fire, which can be assumed to be resting for the moment, in the presence of a forest canopy. This approach therefore builds upon the hitherto known mechanisms of canopy turbulent process and incorporates additional effects of the plume (**Figure 3**), effectively assuming that the fire is a source of buoyancy, provided that the fire is not significantly intense.

Under quiescent conditions, that is, with a very weak ambient wind flow, the most important governing parameter that would determine the plume velocity scale $w_*$ is the strength $B$ of the buoyancy source that represents the fire, assuming that the source geometry is a line. In this framework, the plume angle is defined as

$$\theta_p \approx \frac{dz}{dx} \approx \frac{z_{pc}}{x_{pc}} \approx \frac{w_*}{u_*}, \quad 6.$$

where $z_{pc}$ is the plume rise height, above which the plume becomes approximately horizontal after a distance $x_{pc}$ from the source (the subscript c indicates centerline) (**Figure 3**). $w_*$ and $u_*$ are vertical and horizontal velocity scales, respectively. Raupach (1990) defines them using a dimensional argument that

$$w_* \approx B^{1/3} \Rightarrow w_*^3 \approx B, \quad 7.$$

where

$$B = \int_{-\infty}^{+\infty} w_* g \frac{\Delta T}{T_0} \mathrm{d}x \approx w_* g \frac{\Delta T}{T_0} R_\mathrm{p} \tag{8.}$$

is a buoyancy parameter.

This is the same as

$$\theta_\mathrm{p} \approx \frac{\mathrm{d}z}{\mathrm{d}x} \approx \frac{z_\mathrm{pc}}{x_\mathrm{pc}} \approx \frac{w_*}{u_*} \approx \frac{B^{1/3}}{u_*} \Rightarrow \frac{w_*^3}{u_*^3} \approx \frac{B}{u_*^3} \approx \theta_\mathrm{p}^3. \tag{9.}$$

This implies that the plume angle $\theta_\mathrm{p}$ can be taken as a proxy for the fire intensity and with increased buoyancy, $\theta_\mathrm{p}$ increases, making the plume more vertical; with increasing shear, $\theta_\mathrm{p}$ decreases as the ambient wind tilts the flame toward the ground. It can now be readily seen (using Equation 8) that

$$w_*^3 \sim w_* g \frac{\Delta T}{T_0} R_\mathrm{p} \Rightarrow \frac{w_*^2}{u_*^2} \sim \frac{g R_\mathrm{p}}{u_*^2} \frac{\Delta T}{T_0} \Rightarrow \frac{w_*}{u_*} \sim \sqrt{\frac{g R_\mathrm{p}}{u_*^2} \frac{\Delta T}{T_0}}. \tag{10.}$$

Therefore, we find

$$\theta_\mathrm{p} \approx \frac{w_*}{u_*} \approx \sqrt{\frac{g R_\mathrm{p}}{u_*^2} \frac{\Delta T}{T_0}}. \tag{11.}$$

According to the linear plume rise model (Equation 3), the plume slope is $\theta_\mathrm{p} \approx \delta/\lambda_\mathrm{pc}$. Therefore, we find $\delta/\lambda_\mathrm{pc} \approx \sqrt{\frac{gR_\mathrm{p}}{u_*^2} \frac{\Delta T}{T_0}}$. Using Equations 3 and 11, we obtain

$$f \approx \frac{\delta/R_\mathrm{p}}{\sqrt{\frac{gR_\mathrm{p}}{u_*^2} \frac{\Delta T}{T_0}}}. \tag{12.}$$

Note that Equations 11 and 12 allow us to express and constrain the Raupach (1990) scaling in terms of the nondimensional variables introduced in Section 2.1 and develop a mathematical relationship for the function $f$ that encodes physical processes for the resting buoyant plume.

## 2.3. Scaling Analysis for Moving Fires

In this section, I introduce a dimensionless parameter called the Byram convective number and connect it with the dimensional analysis presented earlier.

**2.3.1. The Byram convective number.** It is evident that the ROS for a moving fire front driven by a predominant wind is primarily governed by the amount of heat transfer toward the unburned fuel elements downwind. This heat transfer is a result of both radiation and convection between the burning zone and the vegetation canopy ahead of the fire front. This net heat transfer can be conjectured to be a result of competing effects from buoyancy-driven effects above the fire plume and the inertia effects from the wind (Pagni & Peterson 1973, Morvan 2011, Morvan & Frangieh 2018). A nondimensional number that encodes this competition in a simplified manner is the Byram convective number $N_\mathrm{c}$, defined as the ratio of the rate of heat release in the vertical direction due to buoyancy effects and the power associated with inertia forces related to the wind flow in the direction of spread (Byram 1959, Nelson 1993):

$$N_\mathrm{c} = \frac{2 g I_\mathrm{B}}{\rho C_\mathrm{p} T_0 (U_\mathrm{w} - \mathrm{ROS})^3}, \tag{13.}$$

where $g$ is acceleration due to gravity, $\rho$ is the density and $C_\mathrm{p}$ is the specific heat of the gas, $T_0$ is the ambient air temperature, $U_\mathrm{w}$ is the mean wind speed, and ROS is the rate of spread. $I_\mathrm{B}$ is defined as the fire-line intensity and can be related to the ROS as

$$I_\mathrm{B} \approx W \cdot H \cdot \mathrm{ROS}, \tag{14.}$$

where $W$ is the weight of fuel consumed per unit area in the flaming zone and $H$ is the heat of combustion of the solid fuel, a material property. It is then evident that when $N_c \gg 1$, the fire is dominated by buoyant plume dynamics and the plume would be nearly vertical. The strong buoyant updrafts would also lead to strong downdrafts of cold air from the surrounding atmosphere, and the heat transfer to downwind fuels would be mainly driven by radiation. On the other hand, when $N_c \ll 1$, the flame would be more tilted toward the horizontal direction and wind-driven convective heat transfer would dominate heat transfer toward unburned fuel (Morvan & Frangieh 2018).

**Fuel moisture content (FMC):** amount of moisture contained in fuel, expressed as the percentage of water over weight of dry fuel

While Byram (1959) considered different fire behavior regimes using different ranges of $N_c$ at the limits of free convection ($N_c > 1$) and forced convection ($N_c < 1$), Clark et al. (1996) described fire regimes using variations of $F_c^2$ as wind driven ($F_c^2 > 1$) or plume or convection driven ($F_c^2 < 1$). Both Byram (1959) and Clark et al. (1996) conjectured that plume- or convection-driven fires are susceptible to more erratic behavior and prone to blowing up, which has obvious practical implications for firefighting. Note that I have demonstrated that both sets of nondimensional numbers can be compared with bulk Richardson number scaling, and therefore they are fundamentally equivalent to the ratio of mechanical and buoyant production mechanisms of turbulence (see the sidebar titled Similarity Between the Byram Convective Number and the Bulk Richardson Number).

**2.3.2. Constraining the Byram convective number.** We use the definition of the Byram convection number given by

$$N_c = 2\frac{gI}{\rho c_p T_0 (U_w - \mathrm{ROS})^3}, \text{ where } B = \frac{gI}{\rho c_p T_0}.$$

$$\text{For a static source, ROS} \to 0, \text{ and } N_c \sim \frac{gI}{\rho c_p T_0 [U]^3}.$$

The fire-line intensity ($I$) can be obtained from Nelson's formula (Sullivan 2007), $I = \dot{m} c_p \Delta T = \rho D w_* c_p \Delta T$, where $\dot{m}$ is the mass flux rate and $D$ is the flame depth. Using these relations, we obtain

$$N_c \sim \frac{gD\Delta T}{T_0 u_*^3} w_* \sim \left[\frac{gD}{u_*^2}\right]\left[\frac{\Delta T}{T_0}\right]\frac{w_*}{u_*} \equiv \left[\frac{gD}{u_*^2}\right]\left[\frac{\Delta T}{T_0}\right]\frac{\delta}{\lambda_{pc}}, \text{ where } D \equiv L_x \equiv R_p.$$

Using Raupach's assumption of $w^3 \sim B$, Sullivan (2007) obtained the relation $N_c \sim F_c^{-3}$, where $F_c$ is the Clark convective Froude number. For a static source, that is, in the limit $r \to 0$, we obtain

$$F_c^{-3} \sim \left(\frac{gD}{u_*^2}\frac{\Delta T}{T_0}\right)^{3/2}.$$

This gives us $N_c \sim \left(\frac{gD}{u_*^2}\frac{\Delta T}{T_0}\right)^{3/2}$, which helps us recover $\frac{\delta}{\lambda_{pc}} \sim \sqrt{\frac{gD}{u_*^2}\frac{\Delta T}{T_0}}$ as before (Equation 11). Moreover, the Byram convection number varies as the cube of the slope of the plume centerline in the rise phase, that is, $N_c \approx Ri_{e_\omega} \approx \left(\frac{\delta}{\lambda_{pc}}\right)^3 \approx \theta_p^3$ (combining Equations 9 and SB4).

Additionally, Morvan & Frangieh (2018) used Equation 13 to express the ROS as

$$\frac{\mathrm{ROS}}{U} \approx F_B(N_c, \mathrm{FMC}), \qquad 15.$$

where $F_B$ is a functional form to be determined from experiments and FMC is the fuel moisture content. It is evident that for strong wind-driven fires ($N_c \ll 1$), $\theta_p \to 0$, and therefore ROS/$U$ is only a function of FMC. This discussion therefore allows us to connect the major scaling relations found in the literature (Byram 1959, Raupach 1990) with each other and with the plume slope for both resting buoyant plumes and moving fires; they are both consistent with the dimensional analysis presented earlier, as well as the effective bulk Richardson number.

## SIMILARITY BETWEEN THE BYRAM CONVECTIVE NUMBER AND THE BULK RICHARDSON NUMBER

The physical interpretation of the Byram convective number $N_c$ is essentially a competition between buoyancy and shear effects, and therefore, we make an attempt to explore its connection with the similar concept of Richardson number ($Ri$), thus connecting it to more fundamental turbulence literature. The bulk Richardson number can be written as

$$Ri_b \approx \frac{g\Delta T}{T_0}\frac{\Delta z}{u*^2}, \tag{SB1.}$$

where $\Delta T$ is the temperature difference between the thermal plume and the ambient air, $\Delta z$ is the measurement height, and $u_*$ is the turbulent friction velocity. This can be further simplified into an effective Richardson number for buoyant plumes:

$$Ri_{e_\smile} \approx \frac{g\Delta T}{T_0}\frac{[L][w]}{[U]^3}, \tag{SB2.}$$

while maintaining dimensional consistency and using $[L]$, $[w]$, and $[U]$ as a length scale of the convection column, vertical velocity scale, and horizontal velocity scale. The length scale $[L]$ can be taken as the flame depth and the velocity scale $[U]$ can be taken as the difference between the mean wind speed and the ROS: $U_w - \mathrm{ROS}$. The fire-line intensity can also be expressed as $I_B \approx \dot{m} C_p \Delta T$, where $\dot{m} = \rho[L][w]$ (Sullivan 2007), therefore reducing Equation 13 into

$$N_c \approx \frac{gI_b}{\rho C_p T_0 [U]^3} \approx \frac{g\rho[L][w]C_p\Delta T}{\rho C_p T_0 [U]^3}. \tag{SB3.}$$

This leads to

$$N_c \approx \frac{g\Delta T}{T_0}\frac{[L][w]}{[U]^3} \approx \frac{B}{[U]^3} \approx Ri_{\mathrm{eff}}, \tag{SB4.}$$

where $B$ can be defined as buoyancy of a fire with a length scale $[L]$: $B = gI_B/\rho C_p T_0$ (Sullivan 2007), which is consistent with Equation 8. Note that Equations SB2 and SB4 are the same, and therefore it can be argued that the Byram criterion can be interpreted as an effective bulk Richardson number.

It is also interesting to note that the bulk Richardson number $Ri_b$ in Equation SB1 is equivalent to the square of an inverse Froude number, also known as the Clark Froude number in the literature (Clark et al. 1996):

$$F_c = \sqrt{\frac{[U]^2}{g\frac{\Delta T}{T_0}[L]}}. \tag{SB5.}$$

**2.3.3. Incorporating vegetation effects within the Byram criterion.** It is evident that the Byram convective number $N_c$ does not account for vegetation canopy characteristics. Zhang et al. (2020) suggested that at least the canopy drag length scale $C_d\mathrm{LAD}^{-1}$ or the height-integrated nondimensional term $C_d\mathrm{LAI}$ is another important dimensionless parameter (LAI is the leaf area index) that should be used alongside $N_c$ to investigate fire plume dynamics over a vegetation canopy at minimum. The dimensional analysis described earlier (Desai et al. 2025b) suggests that a combination of length scales $h_c/(C_d\mathrm{LAI})$, defined as an extinction length scale, is perhaps more appropriate (Morvan 2011). This extinction of momentum inside the canopy can be made dimensionless using $h_c/L_c$.

## 3. MODELING AND GOVERNING EQUATIONS

In this section, I first introduce semiempirical models for fire spread over both grasslands and the canopy and then discuss fully coupled physics-based fire behavior modeling approaches.

**Leaf area density (LAD):** leaf surface area per unit volume of canopy

### 3.1. Empirical and Operational Models for Fire Spread

A number of empirical and semiempirical models can be found that are used as operational fire behavior prediction systems, such as BEHAVE (Burgan & Rothermel 1984), FARSITE (Finney 1998), FlamMap (Finney 2006), and BehavePlus (Andrews 2013). Most of these models use the Byram convective number as an indicator of buoyancy-driven or shear-driven fire regimes, along with a fire spread model developed by Rothermel (1972). A crown fire model was also later developed by Rothermel (1991) based on the original Rothermel (1972) fire spread model. It is notable that the wildland fire module of the Weather Research and Forecasting model [WRF-FIRE (Mandel et al. 2011, Coen et al. 2013)] also uses the Rothermel (1972) model for fire spread.

According to the Rothermel (1972) model (developed based on bench-scale lab experiments), the ROS of a fire is given by

$$R = R_0(1 + \phi_s + \phi_w), \tag{16.}$$

where $R_0$ is the ROS under no ambient wind and on flat terrain, $\phi_s$ is a slope factor, and $\phi_w$ is a wind factor. $R$ is defined as a ratio of heat received by a fuel element from the fire front over the heat required to bring it to ignition [note that it follows from Equation 14 as ROS $\approx I_B/(WH)$]:

$$R_0 = \frac{I_R \xi}{\rho_b \varepsilon Q_{ig}}. \tag{17.}$$

$I_R$ is the reaction intensity, $\xi$ denotes the propagating flux ratio, defined as the proportion of the reaction intensity that heats adjacent fuel particles to ignition under the no-wind scenario, $\rho_b$ is the fuel bulk density, and $\varepsilon$ is called an effective heating number, defined as the proportion of a fuel particle that is heated to ignition temperature at the beginning of flaming combustion. $Q_{ig}$ is the heat of ignition, defined as the amount of heat required to ignite a unit mass of fuel. These variables were then related empirically to fuel particle parameters (heat content, mineral content, dry density), fuel bed properties (surface area to volume ratio, dry weight, bed depth, dead fuel moisture of extinction), and environmental properties (moisture content, wind velocity at midflame height, plume slope). The reader is referred to Andrews (2018) for a detailed discussion of the Rothermel model.

### 3.2. Modeling Crown Fire and Canopy Scorch Damage

A crown fire happens when flames in a wildland fire ignite and/or sustain the burning of the canopy fuel. Given the higher fuel availability, these fires are usually of higher intensity compared to surface fires. The phenomenon associated with the flames ascending up the vertical height of the canopy is called laddering and is often aided by the presence of dry midstory fuels (typically shrubs and brush). When the flames can travel aerially between canopy crowns, it is called crowning. Van Wagner (1977) was the first to systematically study the initiation and spread of crown fires. The canopy scale variables that were identified by Van Wagner (1977) are canopy base height; foliar moisture content, also known as live fuel moisture; and foliar bulk density, which can be related to leaf area density (LAD). Van Wagner (1977) also defined three classes of crown fires—passive, active, and independent—depending on the critical values of three variables—fire intensity at the surface at the beginning, the ROS after crowning begins, and the rate of heat transfer to the unburned fuel downstream.

**Crown scorch:** heat damage of foliage at the higher levels of the canopy

According to Van Wagner (1977), the initiation of the crowning process is dependent on whether a critical temperature at the base of the crown is attained. The difference of this temperature above the ambient temperature can be described as $\Delta T \propto I_B^{2/3}/z$ or $\Delta T = k_c I_B^{2/3}/z$, where $k_c$ is a crown scorch proportionality factor with the unit of $°Cm^{5/3}kW^{-2/3}$ (Michaletz & Johnson 2006), varying between 4.5 and 9 for different tree species. This 2/3 scaling relation is based on buoyant plume theory developed using line fire experiments by Thomas (1963), and flame length is often assumed to be proportional to $I_B^{2/3}$. $I_B$ is still defined as the Byram intensity given by Equation 14. The heat of ignition $h$ is assumed to depend mainly on the foliar fuel moisture. Using empirical arguments, Van Wagner (1977) defined a critical intensity of the fire at the surface to initiate crowning $I_0 = (Czh)^{3/2}$, where $C$ is another empirical constant with appropriate dimensions and obtainable from experimental data. The necessary condition for the onset of crown combustion is therefore given as $I \geq I_0$.

The next step after initiating the crown fire is the spread from crown to crown, and to define the conditions for crown spread, a net horizontal heat flux $E$ is defined as $E = \text{ROS} \cdot d \cdot h$, where $d$ is the bulk density of the canopy fuel in accordance to Thomas (1963). It is noted that this equation is similar to Equation 14 and $d$ and $h$ are now defined as canopy-scale variables, instead of being properties of individual trees. This equation can be rearranged as $Rd = E/h = S$, or $R = S/d$, where $S$ can be defined as a mass flow rate of fuel into the crown space in the units of mass per unit cross section per unit time. This is conceptualized as a conveyor belt model where the fire front is assumed to be fixed in space and the fuel is flowing horizontally into it through a vertical cross section. It is then conjectured that below a critical mass flow rate $S_0$ and an associated ROS $R_0 = S_0/d$, the crowning cannot be sustained.

Therefore, to summarize Van Wagner (1977), laddering happens when $I \geq I_0$. Horizontal spread of crown fire will happen when $E$ exceeds a critical number $E_0$ and $S \geq S_0$. A passive crown fire occurs when $I \geq I_0$ but $R \leq R_0$, and an active crown fire happens when $I \geq I_0$ and $R \geq R_0$. An independent crown fire happens when $I \geq I_0$, $R \geq R_0$, and $E_0$ is supplied entirely by the canopy crown.

The Van Wagner model is evidently highly empirical, and Michaletz & Johnson (2006) proposed a revised model of crown scorch in the zone of influence of a convective plume above a surface fire of moderate intensity.

It is also worth noting that using computational simulations, it is possible to identify scenarios susceptible to scorch damage (Atchley et al. 2024). For example, Banerjee (2020) and Banerjee et al. (2020a) identified that under low fuel moisture conditions, the sensible heat flux from a surface fire in a thinned forest could be higher compared to the nonthinned forest, because of higher turbulence intensity near the surface. More work is therefore needed to connect empirical crowning models with physically based models for heterogeneous canopy fuel structures.

## 3.3. Governing Equations for Physics-Based Models

All physically based fire behavior models have fundamental similarities. To solve for the coupled dynamics between the vegetation and the surrounding atmosphere, two sets of equations are written, one for the solid fuel elements and one for the gas phase. The solid phase equations can be summarized as conservation equations for fuel mass, moisture, and energy, assuming a thermally thin material, that is, locally homogeneous distributions of temperature within the fuel elements. The equations for the gaseous phase include conservation equations for mass, momentum, and energy, with a double averaging procedure now standard in the canopy turbulence literature (Finnigan 2000, Nepf 2012); this homogenizes the net effect of the interaction between the air and from small-scale vegetation elements such as individual leaves, branches, and twigs into an average representative drag effect (Linn & Cunningham 2005, Morvan 2011) (see the sidebar titled Revisiting the Theory of Combustion).

## REVISITING THE THEORY OF COMBUSTION

The basic fluid mechanics of combustion is well-understood (Tieszen 2001) and not discussed in detail in this work. The simplest equation for combustion can be written as fuel + oxygen = products + heat (Faraday et al. 1920). A fire is essentially an uncontrolled chemical oxidation of organic fuels, and the heat of combustion sustains the controlled burning of adjacent organic fuels. This process can be described by Arrhenius-type equations that describe the reaction rate based on kinetic theory:

$$\dot{\omega} = A Y_f^n Y_O^m exp(-E/RT), \quad \text{SB6.}$$

where $A$ is a rate constant, $Y_f$ and $Y_O$ are fuel and oxygen concentrations, $n$ and $m$ are reaction orders, $R$ is the gas constant, $T$ is the temperature, and $E$ is the activation energy. The energy released per unit time and unit volume from the reaction is given by

$$\dot{Q} = \rho \Delta H_c \dot{\omega}, \quad \text{SB7.}$$

where $\rho$ is the bulk density of the reactants and $\Delta H_c$ is the heat of combustion or the energy produced per unit mass of the fuel. This energy released $\dot{Q}$ is partly transferred back to the fuel and partly lost to the environment. The fraction of this energy transferred back to the fuel will define the flame temperature $T_F$. If $T_F$ is high enough, then enough heat is transferred to fresh reactants, leading to a self-sustained reaction. If $T_F$ is too low, then an external energy supply is necessary to sustain the combustion. In wildland fires, the fuel and oxygen need to be transferred to the reaction zone, which is governed by turbulent diffusion, and therefore, wildland fire flames are called diffusive flames.

During the chemical reaction, the solid fuels also change phase, which is called pyrolysis. The rate of pyrolysis is defined by an equation similar to Equation SB6. Once enough fuel is produced, a flammable mixture is produced in the gas phase, and the combustion can proceed. The heat feedback from the flames will sustain the reaction as discussed above if enough fuel is produced. This process is encoded in the mass transfer number

$$B_m = \dot{Q}_{feedback}/\dot{Q}_{pyrolysis}. \quad \text{SB8.}$$

It is evident that for a self-sustaining reaction, the necessary criterion is $B_m > 1$. The role of canopy turbulence during an active fire is therefore producing $B_m > 1$ as a result of the turbulent heat and mass transfer processes around the fire front.

The phenomenon of fuels undergoing a chemical reaction during combustion can be represented at a minimum as a single compartment model as (Linn & Cunningham 2005)

$$N_f + N_O = (products) + (heat), \quad 18.$$

where $N_f$ and $N_O$ are stoichiometric coefficients for fuel and oxygen. This approach combines pyrolysis and gaseous combustion into a single simplified combustion model instead of tracking the transport of individual species, with the argument that within a relatively coarse grid size (of the order of 1 m), the subgrid scale variability of transport and mixing can be ignored and lumped together, essentially assuming that the pyrolysis and combustion happen within the same location. This is the approach taken by the FIRETEC model (Linn & Cunningham 2005, Linn et al. 2005), while other models such as FIRESTAR3D (Morvan 2011) and WFDS (Wildland–Urban Interface Fire Dynamics Simulator) (Mueller et al. 2014) track budgets for individual species during the combustion.

**Pyrolysis:** thermal decomposition of organic material in the absence of oxygen, a precursor to combustion

The equations for the solid phase can be written as

$$\frac{\partial \rho_f}{\partial t} = -N_f F_f, \quad 19.$$

$$\frac{\partial \rho_w}{\partial t} = -F_w, \tag{20.}$$

**Heat feedback:** process by which heat from the fire is transferred back to unburned fuel

$$\left(c_{pf}\rho_f + c_{pw}\rho_w\right)\frac{\partial T_s}{\partial t} = Q_{rad,s} + C_h a_v\left(T_g - T_s\right) - F_w\left(H_w + c_{pw}T_{vap}\right) + F_f\left(\Theta H_f - c_{pf}T_{pyr}N_f\right). \tag{21.}$$

Equations 19 and 20 track the loss rate of the densities of solid vegetation fuel mass and the water contained within that fuel due to the combustion process, where $\rho_f$ denotes the solid fuel density and $\rho_w$ denotes the bulk density of liquid water. $F_f$ denotes the reaction rate of solid vegetation fuel and $F_w$ denotes the reaction rate for liquid water loss. Equation 21 tracks the temperature of the solid vegetation fuel, which is dependent on the heat received by radiation (first term on the right-hand side) and convection (second term on the right-hand side), heat loss due to the vaporization of fuel moisture (third term on the right-hand side), and a balance between the heat loss from pyrolysis and the heat feedback onto the solid surface (fourth term on the right-hand side). $c_{pf}$ and $c_{pw}$ denote the specific heats at constant pressure for fuel and water. $T_s$ is the solid fuel temperature. $Q_{rad,s}$ is the net thermal radiation flux to the solid. $C_h$ denotes the convective heat transfer coefficient. $a_v$ denotes the surface area to the resolved volume ratio, calculated as the surface area per unit volume of fuel times the volume fraction. $T_g$ denotes the temperature of the combined gas phase. $H_w$ is the heat energy per unit mass from the evaporation of liquid water. $T_{vap}$ is the temperature of evaporation of liquid water. $H_f$ denotes the heat energy per unit mass for the reaction denoted by Equation 18. $\Theta$ is the fraction of heat released from the bulk solid–gas reaction given by Equation 18 that is deposited back to the solid. $T_{pyr}$ is the temperature at which the pyrolysis of the solid fuel begins (Linn & Cunningham 2005).

The equations for the gas phase can be summarized as

$$\frac{\partial \rho_g}{\partial t} + \frac{\partial}{\partial x_j}\left(\rho_g u_j\right) = N_f F_f + F_w, \tag{22.}$$

$$\frac{\partial}{\partial t}\left(\rho_g u_i\right) + \frac{\partial}{\partial x_j}\left(\rho_g u_i u_j\right) = -\frac{\partial p}{\partial x_i} - \frac{\partial R_{ij}}{\partial x_j} - \rho_g C_D a_v |u| u_i + \rho_g g_i, \tag{23.}$$

$$\frac{\partial}{\partial t}\left(\rho_g \theta\right) + \frac{\partial}{\partial x_j}\left(\rho_g \theta u_j\right) = \frac{\partial}{\partial x_j}\left(\sigma\frac{\partial \theta}{\partial x_j}\right) + \frac{\theta}{c_p T_g}\left[C_h a_v\left(T_s - T_g\right) + Q_{rad,g} + (1-\Theta)F_f H_f\right], \tag{24.}$$

$$\frac{\partial \rho_o}{\partial t} + \frac{\partial}{\partial x_j}\left(\rho_o u_j\right) = \frac{\partial}{\partial x_j}\left[\sigma\frac{\partial}{\partial x_j}\left(\frac{\rho_o}{\rho_g}\right)\right] - N_o F_f, \tag{25.}$$

where Equation 22 denotes the conservation of mass, Equation 23 denotes the momentum budget, and Equation 24 denotes the temperature budget for the bulk gaseous phase. $\rho_g$ denotes the bulk gas density and $u_i$ denotes the gas velocity in standard tensor notation, where $i = 1, 2, 3$ denotes the velocity components in the $x$, $y$, or $z$ directions. $g$ is the acceleration due to gravity, $R_{ij}$ is the Reynolds stress tensor, $C_D$ is the canopy drag coefficient, $\theta$ is the potential bulk temperature of the combined gas phase, $\sigma$ is the turbulent diffusion coefficient, and $c_p$ is the specific heat of the combined gas phase at constant pressure. $Q_{rad,g}$ is the radiation heat flux to the gas and $\rho_o$ is the density of oxygen. For modeling of the turbulent stress, readers are referred to Linn & Cunningham (2005) and Linn et al. (2005).

Other physics-based models, such as WFDS (Mueller et al. 2014), use a similar approach to the Navier–Stokes equation with a canopy drag in a large eddy simulation (LES) framework. A momentum budget equation is written for the mass-weighted Favre filtered velocity components,

which is standard in the canopy turbulence literature (Shaw & Schumann 1992). The modeling of the deviatoric stress tensor is then modeled using a turbulent eddy viscosity (Deardorff 1980):

$$\nu_t \approx \Delta\sqrt{k_{sgs}}, \qquad 26.$$

where $k_{sgs}$ is the subgrid scale turbulent kinetic energy (TKE). Other models, such as ARPS-CANOPY (Kiefer et al. 2013), use a TKE budget equation for the $k_{sgs}$. Bebieva et al. (2020) developed a formulation for the horizontal eddy viscosity for heat transfer in a forest canopy using an advection–diffusion–reaction equation and evaluated it against field experimental data. The reader is also referred to Grishin (1996) for additional self-contained model formulation.

**Trough:** finger-like region at the flame front characterized by vertical velocity downdrafts

**Tower:** finger-like region at the flame front characterized by vertical velocity updrafts

## 4. KEY FEATURES OF FIRE–CANOPY TURBULENCE AND COHERENT STRUCTURES

In this section, I discuss key features of canopy–fire–atmosphere interaction. For additional details on the nature of flow organization via coherent structures, details of flow statistics, the nature of turbulent energy generation and transport, the impact of canopy structure and landscape heterogeneity, and the intermittent nature of fire propagation in forest canopies, readers are referred to the **Supplemental Appendix**, section 5.

Supplemental Material >

### 4.1. Impact of Wind Speed on Fire Front Propagation

While bulk relations between the fire ROS and buoyancy flux have been established in Section 2, the intricate relationship between fire-line geometry, ROS, and wind speed and turbulence can be further investigated using numerical simulations of the coupled fire–vegetation–atmosphere interaction. Linn & Cunningham (2005) and Cunningham & Linn (2007) observed that while the bulk relation of increasing ROS with increasing wind speed observed in the scaling analysis and empirical models holds up, the ROS is also a function of the initial length of the ignited fire line ($Fl_l$) (**Figure 4**). For the same ambient wind speed, the ROS for long fire lines is higher than that of shorter fire lines. In addition, the ROS in the lateral direction (called the flanking part of the fire perimeter) is also a function of the wind speed and $Fl_l$. For weak ambient winds, the shape of the fire perimeter changes significantly with changing wind speeds.

For a fixed length of the fire line, an increased wind speed leads to more tilted flames, increasing the ROS. At a significantly high wind speed, the fire perimeter appears as a double ellipse as observed by several experiments (Fons 1946) and becomes less sensitive to the rate of change of the wind speed (as we observed in Equation 15). For wind-driven fires, the highest wind speed along the streamwise direction is observed right behind the fire front (**Figure 4*d***), which is associated with less drag and also enhanced by an indraft of cold air from the surrounding area. With increasing wind speed, there is enhanced advective heating of the fuel elements downstream, as the ambient wind can penetrate through the buoyant plume through the trough regions (zones of downdraft between towers of updraft regions, which organize the flame front) (**Figure 4*a*,*b*,*e***). Moreover, at higher wind speeds, with an increasingly tilted flame (low $\theta_p$), the radiative heating of the unburned fuel ahead is also enhanced. The pressure perturbations due to the buoyant plume lead to the entrainment of cold air from the surrounding regions, and the inflow of cold air at the base of the buoyant plume could also lead to a reversal of the wind flow at the unburned fuel downstream and lead to convective cooling, reducing the ROS. This entrainment effect in the weaker wind speeds would not permit significant spread in the lateral direction, which leads to different shapes of the fire perimeter in higher wind speeds (**Figure 4*a*,*b***).

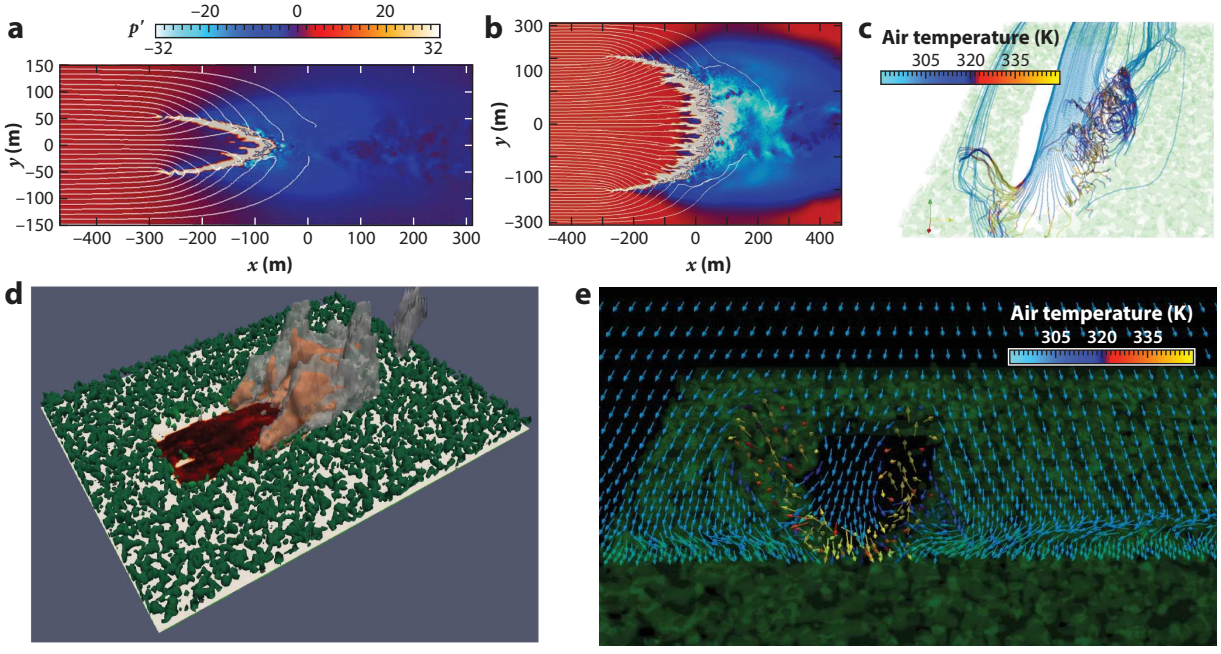


**Figure 4**

Role of the wind. (*a*, *b*) Graphs showing pressure perturbations and streamlines for a (*a*) short and (*b*) long line of fire. (*c*) FIRETEC simulation of streamlines surrounding a fire perimeter showing helical patterns. (*d*) Typical FIRETEC simulated moving flame in a complex three-dimensional forest structure. (*e*) A vertical plane showing wind vectors colored by air temperature, perpendicular to the direction of wind flow and fire spread, as the fire progresses toward the reader. Note the counterrotational vortices on the two flanks of the fire and the induced flow above and through the forest canopy from the left and right edges toward the fire front, demonstrating wildland fire entrainment. Panels *a* and *b* adapted with permission from Canfield et al. (2014).

## 4.2. Impact of Fire Configuration and the Role of Entrainment

The buoyant plume column acts like a barrier to the ambient wind flow, and some parts of the flow go around the column. The strength of this buoyancy increases with the fire intensity. This structure is associated with an intensification of pressure at the fire perimeter, a low-pressure region downwind, and therefore a net negative pressure gradient from the upwind side to the downwind side of the fire (Canfield et al. 2014). The nature of this pressure gradient for both short and long fire lines leads to different flow patterns around the fire line (**Figure 4*a*,*b***). With a high wind speed, for a shorter fire line, the negative pressure outside the flanking region on both sides leads to more streamlines diverging to these areas and fewer streamlines available to impinge through the fire front. This leads to a more conical shape of the fire front. With a longer fire line, the competition from the flanking sides is weaker and more streamlines are available to impinge through the fire front.

The entrainment flux of cold air from the surrounding air at the base of the plume sustains the buoyant column (**Figure 4*c*,*e***). For shorter fire lines, this means that during weaker ambient flow, more of the ambient flow is entrained into the column rather than going around it, and there is less penetration of the ambient wind through the column to carry advective heating to the unburned fuel. For stronger wind speeds with a short fire line, more ambient flow is redirected around the buoyant column rather than being entrained into it, and there is more advective heating through the fire front, leading to more lateral spread and a necking of the fire perimeter.

With a longer fire line, the buoyant plume acts as a more widespread barrier (not a solid barrier, of course, since the air can be entrained into it or penetrate through) to the ambient wind. For weaker wind speed, the lateral spread is negligible, similar to shorter fire lines. This entrainment is sustained by counterrotating vortex pairs (CVPs) on the two sides of the plume base (**Figure 4*c*,*e***). With increasing wind speeds, most of the flow is forced to impinge through the plume, increasing advective heating and the ROS.

The flow of near-surface air from surrounding areas into the zone of combustion, because of the pressure gradients due to the buoyant plume, is generally characterized as wildland fire entrainment (WFE) (Linn et al. 2025). This entrained air flow is therefore nonlocal and sensitive to the heterogeneities in the environment surrounding the fire, for example, variations in the fuel structure, complex terrain, fuel breaks, and so on. This WFE therefore encodes the nonlocal impact of the surrounding areas on fire behavior. In **Figure 4*c*,*e***, this entrainment phenomenon is illustrated clearly. In **Figure 4*c***, the entrained air from the surrounding area joins at one of the CVPs in a helical fashion, which is also confirmed in experimental data (Desai et al. 2022). In **Figure 4*e***, the two-dimensional plane shows the entrainment flow from the two sides joining at the base of the CVP. It can therefore be stated that modifying the canopy fuel structure in the vicinity of the fire front could impact fire behavior and thereby offer an opportunity in the context of fuel treatment and firefighting.

### 4.3. Tower–Trough Structures

It has long been recognized that a moving fire front over a bed of fuel is not a solid interface (a sheet of flame or a wall of flame) that can be described as a two-dimensional flow, but rather a three-dimensional structure (**Figure 5*a***) comprised of peaks (or towers) and troughs (Finney et al. 2015), as initially discussed by Beer (1991). These structures are not associated with the structure of the fuel bed but rather with the thermal instability, and because of this, it is difficult to define a unique flame height as these peaks and troughs meander, oscillate, and move around in time and space. The towers are regions of updraft, and the troughs between the towers are regions of downdraft; this finger-like organization is a consequence of the combined motion of simultaneous warm updrafts and cold downdrafts associated with the fire front. The ambient wind can pass through these troughs, and this describes the genesis of the so-called fire wind. Beer (1991) also identified that these sweeps of cold air from aloft would push the flame into the canopy fuel bed and preheat the fuel downstream through advection. These sweeps, of course, are the same as the sweep–ejection sequences associated with canopy turbulence (Finnigan 2000) and are discussed later. For now, it is sufficient to mention that the sweeps are associated with turbulent wind fluctuations rather than the mean wind speed and apart from enhancing the advective preheating of the unburned canopy fuel, they also introduce the aspect of intermittency and burstiness associated with fire spread, all of which are not accounted for in a typical ROS analysis using mean variables.

Banerjee et al. (2020b) used numerical simulations using FIRETEC to quantify the tower–trough structures (**Figure 5*b***) and also identified that the troughs are associated with higher oxygen concentration, which is intermittently entrained by the cold sweeps, enhancing the burst of advecting preheating. The statistics of the tower–trough structures were also found to be sensitive to fuel depth and wind speed, evidently as these factors would alter the sweep–ejection dynamics with the canopy as well (Banerjee et al. 2020b). While the tower–trough structures are found in the vertical plane, another type of instability at the fire front (in the horizontal plane) is also observed; it is called viscous fingering. Harris & McDonald (2022) explained this instability at the interface between the burned and unburned fuel, as a result of the curvature of the fire front interface and the concentration of oxygen, using the Péclet number (the ratio of advective to

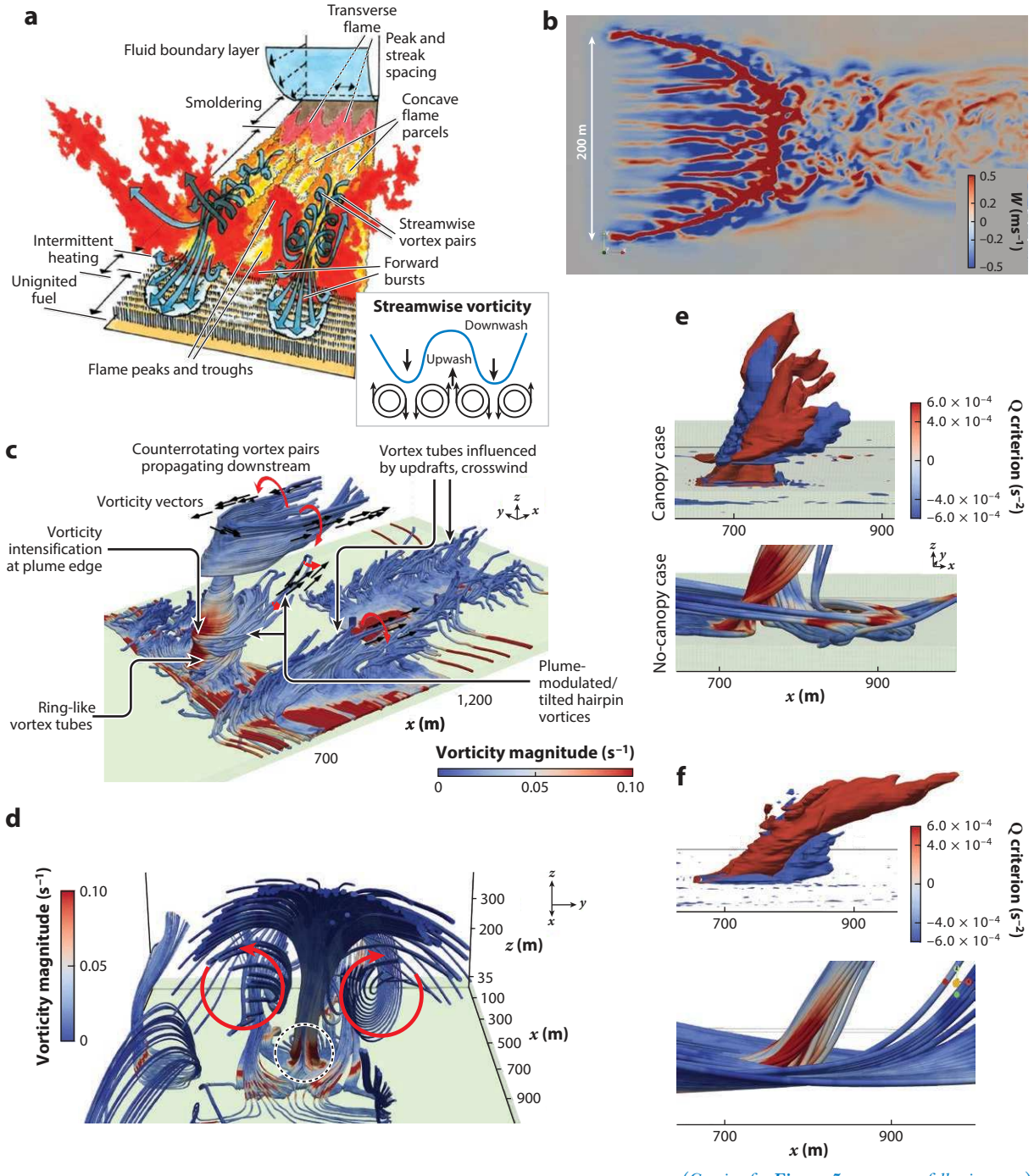


(*Caption for* ***Figure 5*** *appears on following page*)

**Figure 5** (*Figure appears on preceding page*)

Coherent structures and counterrotational vortices associated with fire spread. (*a*) Diagram of the main mechanism of buoyant flume dynamics as well as the tower–trough structures (*inset*) in a fuel canopy. Panel adapted from Finney et al. (2015) (CC BY 4.0). (*b*) A plan view of finger-like tower (*red*)–trough (*blue*) structures on the fire perimeter colored by vertical velocity. Panel adapted from Banerjee et al. (2020b) (CC BY 4.0). (*c*) Vortex tube structures for the buoyant plumes over the canopy with additional details. (*d*) Streamlines from static buoyant plume simulations over a forest canopy, highlighting counterrotating vortices. (*e*) Close-up view of the streamlines for buoyant plume simulations with a forest canopy, with the top showing the Q criterion (the *red* region is rotation dominated and the *blue* region is shear dominated). (*f*) Close-up view of the streamlines for buoyant plume simulations with no canopy, with the top showing the Q criterion (the *red* region is rotation dominated and the *blue* region is shear dominated). Panels *c–f* adapted from Desai et al. (2025a).



diffusive transport). Since the advection of oxygen at the fire front is also dependent on the tower–trough structures, it is possible that the viscous fingering phenomenon is related to tower–trough phenomena; however, more research is needed into this topic.

## 4.4. Counterrotational Vortex Pairs

Finney et al. (2015) refined the conceptual picture of tower–trough structures (**Figure 5*a*,*b***) using video observations of laboratory and field-scale fires and identified that these towers and troughs are associated with sequences of CVPs, as discussed earlier (see the inset in **Figure 5*a***). These CVPs are not planar features either, but join together as helical structures (**Figure 4*c***). The sweeping motions burst through the trough regions intermittently downward and forward, providing the aforementioned advective preheating. This intermittent puffing of the wind as it moves forward through the flame is characterized by a correlation between the Strouhal number $f[L]/[U]$ and the Froude number $Fr^2 = [U]^2/([L]g)$, where $[L]$ and $[U]$ are appropriate length and velocity scales. Desai et al. (2022) used particle imaging velocimetry experiments on small-scale surface fires and confirmed the presence of and quantified the magnitude of these CVPs, as well as the helical nature of the streamlines at the fire front. It is interesting to note that CVPs are also observed with fires that are not wind driven, but they are features of the flow itself, as is the case with the surface fire studied by Desai et al. (2022). The CVPs on either side of the fire front push the hot gases outward, resulting in advective heating and expanding the circular fire perimeter in the absence of an ambient wind. Desai et al. (2025a) conducted LES of resting buoyant plumes and also observed the CVPs on either side of the plume structure (**Figure 5*c–f***), which is similar to what is observed in **Figure 4*e*** from LES simulations of moving fires using FIRETEC. This implies that CVPs are associated with the organization of updraft and downdraft characteristics of the wind associated with the presence of a surface heating anomaly, rather than the feature of moving fires. Desai et al. (2025a) also observed a fundamental difference between the CVP structures for canopy versus no-canopy cases (**Figure 5*e*,*f***). When the plume base is situated within a forest canopy, the canopy drag induces a recirculation at the plume base, which modifies the CVP structure and makes the plume more vertical compared to the no-canopy case. The Q criterion plot reveals the structure, inclination, and extent of the CVPs on either side of the plume. **Figure 5*c*** highlights additional structural features of the CVPs along with other coherent features such as hairpin vortices, which are also tilted along the main wind direction. For a more detailed discussion on vortical features in wildland fires, the reader is referred to Forthofer & Goodrick (2011) and Tohidi et al. (2018).

## 4.5. Sweep–Ejection Dynamics

As evident from the preliminary discussion of coherent structures, sweeps, ejections, and inward and outward interactions are also significant mechanisms as they influence fire spread through both surface and canopy fuels (**Figure 6**). Several field studies (Clements et al. 2007, 2019,

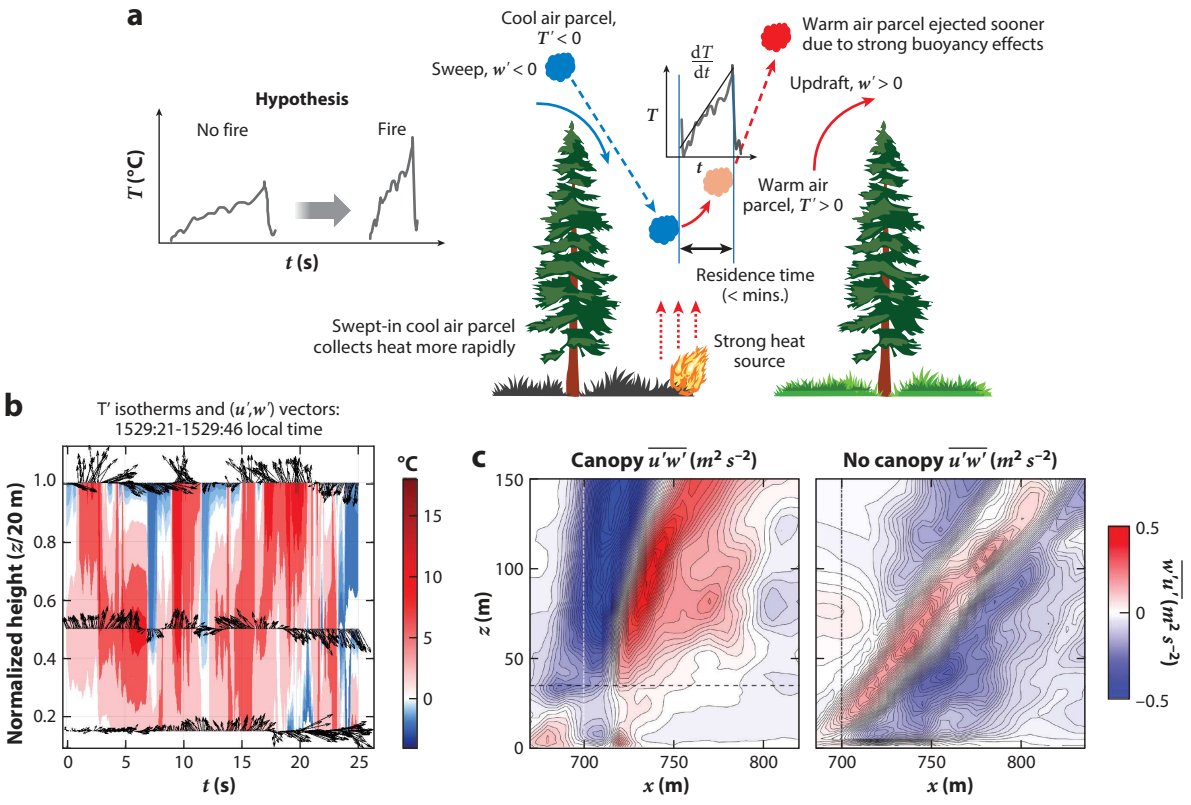


**Figure 6**

Sweep–ejection dynamics for wildland fires within a forest canopy. (*a*) A conceptual picture of the heat transfer process driven by sweeps and ejection sequences with the canopy. Panel modeled after concepts presented in Katul et al. (2013). (*b*) A time–height snapshot plot of temperature isotherms within the canopy airspace with wind vectors at three different heights from field experimental data. Panel adapted from Desai et al. (2024) (CC BY 4.0). (*c*) The vertical momentum flux from static buoyant plume simulations with and without a forest canopy. The blue regions indicate cogradient motions (sweep and ejection) and the red regions indicate countergradient motions (inward and outward interactions). Panel adapted from Desai et al. (2025a).

**Countergradient motion:** turbulent transport occurring opposite to the direction of the mean gradient

Heilman 2021, Heilman et al. 2021) have been conducted in the last few decades to quantify these coherent structures associated with heat and momentum flux events over grassland and forested environments, with different fire configurations such as heading fires (fires moving along the wind direction) and backing fires (fires moving against the wind). Significant differences can be observed in the event fraction and event contribution statistics across heights before, during, and after the fire front propagation. Before fire front propagation, these statistics are consistent with what is typically found in the canopy turbulence literature, which is a higher frequency of sweeps and ejection-type motions (Katul et al. 2013). However, during the fire front passage, the frequency of countergradient motions is found to be enhanced for all cases. More specifically, the frequency of downward flux of warm air from above and upward flux of high horizontal momentum air from below is found to be enhanced for grassland and forested environments (Heilman et al. 2021).

Regarding the event contributions, during fire front propagation, ejections significantly dominate the heat flux events. However, for the vertical momentum flux, it is perhaps a nontrivial finding that sweeps, that is, downward flux of high-momentum air from aloft, dominate near-surface vertical momentum transfer, although the fire environment is supposedly characterized

by strong buoyancy (Heilman et al. 2021). This again highlights the fact that the fire front involves not just upward movement of warmer air above the flame, but a complex organization of warm updrafts and cold downdrafts in tandem and in sequence, which also is the key mechanism for fire spread, as the sweeps tilt the flame forward, enhancing advective preheating. This has implications for smoke ventilation and turbulent energy redistribution within the canopy.

**Cogradient motion:** turbulent transport occurring along the direction of the mean gradient

Further insights into the nature of flow organization through the sequence of sweeps and ejections were uncovered by Desai et al. (2023, 2024). Drawing on similarities with the mechanism (Gao et al. 1989) of scalar exchange between the forest canopy and the atmosphere, Desai et al. (2024) hypothesized that as a sweeping motion brings a cold air parcel from aloft into the forest canopy, it starts to collect heat from the presence of the fire below (**Figure 6*a*,*b***). This leads to a fast increase of the temperature of the air parcel, and once it warms up sufficiently, due to buoyancy effects, it is swept from inside the canopy in an ejection-type motion, leading to very rapid drop in the temperature of the space inside the canopy previously occupied by the air parcel. This sequence of motion manifests into a ramp–cliff-type structure in the air temperature inside the canopy (shown at the top of **Figure 6*a***). The hypothesis was tested using field experimental data collected during heading fires below a forested canopy, and the statistics of the ramp–cliff structures were extracted. It was indeed discovered that the ramp slope is much steeper and the ramp duration is shorter compared to no-fire scenarios. The cliff slope and duration are also steeper and shorter, respectively, compared to no-fire scenarios, and they are shorter and steeper compared to the ramps, indicating that the downdraft motions are stronger. However, these statistics are also sensitive to the location with respect to the bent plume structure within the canopy airspace (Desai et al. 2024).

It is worth noting that using the surface renewal theory (Paw U et al. 2005) (a standard approach in flux estimation in canopy turbulence), the heat flux $\rho C_p \overline{w'T'}$ associated with the fire plume can be estimated using the ramp slope as

$$H_{\text{ramp}} \approx \rho C_p \frac{\partial T}{\partial t} h_c, \qquad 27.$$

where $\partial T/\partial t$ are the ramp slopes that can be extracted from the temperature time series. Desai et al. (2024) estimated that $H_{\text{ramp}}$ is comparable to the $\rho C_p \overline{w'T'}$ measured directly under the influence of fire, and the comparison is worse for no-fire scenarios, especially at lower heights. This implies that the structure of the temperature time series encodes a significant amount of information about the interaction of fire with canopy turbulence. Moreover, this comparison improves at the proximity of the flame and worsens farther away, offering new types of measurement strategies.

LES simulations of resting buoyant plumes by Desai et al. (2025a) and Cervantes et al. (2025) also highlight that during fires, while sweeps and ejections (cogradient motions) remain significant, the countergradient motions, that is, inward and outward interaction events (which are associated with net upward movement of the momentum flux $\overline{u'w'}$), are strengthened significantly compared to no-fire scenarios (**Figure 6*c***). This is also confirmed by field experimental data (Heilman et al. 2021), and it is perhaps due to the fact that without fires, the canopy is mainly an extended sink of momentum for the high-momentum wind aloft (thereby sweeps and ejections dominate net downward $\overline{u'w'}$). However, during a fire front propagation, there is also momentum injection from the bottom of the canopy sublayer (CSL), as observed in **Figure 6*c***. It is interesting to note that the countergradient motions are stronger for the canopy case, compared to the no-canopy case, which makes the plume more vertical for the canopy case. Also, notice that the interface between the cogradient and countergradient motions roughly marks the plume centerline. **Figure 6*b*** shows the structure, duration, depth, and extent of these coherent structures along with the temperature microfronts within the CSL volume.

## 5. CONCLUSIONS AND IMPLICATIONS

This review organizes key processes associated with wildland fire spread in grassland and forested environments over a flat terrain under the thematic umbrella of canopy turbulence. Different aspects of the fluid mechanical processes at different stages of fire behavior can inform different communities, including ecologists, hydrologists, atmospheric scientists, and engineers. The early development of the field has been through lab and field-scale experiments, which led to empirical relationships between environmental variables, such as wind speed and the ROS of fires. More recent computational modeling and detailed turbulence measurements during controlled burns have now revealed more details regarding the key processes that govern fire spread. Nondimensional parameters such as the Byram convective number that are used in the wildland fire literature have been connected with well-established parameters in the turbulence literature, such as the Richardson number, which can be used to describe the competition between shear and buoyancy effects that influence fire spread. A generalized dimensional analysis has been provided, which can be used to constrain major available scaling relationships regarding wildland fire spread. Both empirical and process-based models for describing a moving fire front in a forest have been discussed, as well as the conditions for canopy crown damage and the turbulent coherent structures associated with the fire front and their interactions with canopy turbulence. Finally, the nature of flux and energy transport and turbulent intermittency within the canopy environment during fire spread has been discussed (see the **Supplemental Appendix**), as well as the role of canopy structural heterogeneity on wildland fire spread.

Supplemental Material >

There are several implications of this process-level understanding. The nature of turbulence flux and energy transport within the forest canopy sets up the boundary condition for ember particles and smoke ejections into the atmosphere, as well as their short- and long-range transport. The understanding of how fire propagation is sensitive to small-scale structural variations in the canopy can lead to better designs for prescribed fire, air quality impact management, and fuel treatment scenarios, as well as better mitigation and adaptation against extreme wildfire events.

### SUMMARY POINTS

1. The plume tilt angle is a useful response variable that can be connected to competition between shear and buoyancy.
2. The fire front is organized into a series of updraft and downdraft zones, which are underpinned by counterrotating vortex pairs.
3. The coherent structures associated with fire–vegetation–atmosphere interaction are connected to the sweep–ejection dynamics in canopy sublayer flows.
4. The interplay of buoyant plumes, canopy drag, and fire-induced entrainment impact fire behavior and spread.

### FUTURE ISSUES

1. How does a fire interact with heterogeneities in canopy structure on complex terrain? More experimental data are required to make progress.

2. Modern data acquisition techniques such as ground and uncrewed aerial vehicle–based lidar can create digital twins of canopy structure in very high resolution. How can this detailed information be incorporated into fire behavior models?
3. How does the canopy microclimate change with forest thinning; for example, how does it affect live fuel moisture? There is contrasting information on this topic in the literature, and more experimental data are required.
4. Certain fire-adapted tree species release seeds during wildland fires. The dispersion patterns of seeds by the fire wind determines future postfire ecological succession and requires further investigation.
5. More accurate predictions of live fuel moisture are required for fire behavior modeling that takes the canopy turbulent processes into account.
6. How the forest canopy intercepts dropped water or fire retardants from moving air tankers is important for aerial firefighting, and better understanding of this process is required to improve the efficiency of these drops.

## DISCLOSURE STATEMENT

The author is not aware of any affiliations, memberships, funding, or financial holdings that might be perceived as affecting the objectivity of this review.

## ACKNOWLEDGMENTS

I acknowledge funding support from the US National Science Foundation (NSF-AGS-PDM-2146520, NSF-OISE-2114740, NSF-CPS-2209695, NSF-ECO-CBET-2318718, NSF-DMS-2335847, and NSF-RISE-2536815), the University of California Office of the President (UCOP-LFR-20-653572), NASA (80NSSC22K1911), and the United States Department of Agriculture (NIFA 2021-67022-35908, and USDA-20-CR-11242306-072). I acknowledge my PhD students and postdoctoral scholars at the University of California, Irvine, for their support, especially Ajinkya Desai for help and discussions. I also acknowledge a visiting fellowship from the Institute of Advanced Studies, University of Surrey, UK, which supported my sabbatical during the fall of 2024.

## LITERATURE CITED

Accary G, Sutherland D, Frangieh N, Moinuddin K, Shamseddine I, et al. 2020. Physics-based simulations of flow and fire development downstream of a canopy. *Atmosphere* 11(7):683

Albini FA. 1985. A model for fire spread in wildland fuels by-radiation. *Combust. Sci. Technol.* 42(5–6):229–58

Albini FA, Alexander ME, Cruz MG. 2012. A mathematical model for predicting the maximum potential spotting distance from a crown fire. *Int. J. Wildland Fire* 21(5):609–27

Andrews PL. 2013. Current status and future needs of the BehavePlus Fire Modeling System. *Int. J. Wildland Fire* 23(1):21–33

Andrews PL. 2018. *The Rothermel surface fire spread model and associated developments: a comprehensive explanation.* Tech. Rep. RMRS-GTR-371, Forest Service, US Department of Agriculture

Arreola Amaya M, Clements CB. 2020. Evolution of plume core structures and turbulence during a wildland fire experiment. *Atmosphere* 11(8):842

Atchley AL, Hoffman CM, Bonner SR, Ritter SM, O'Brien J, Linn RR. 2024. Evaluating crown scorch predictions from a computational fluid dynamics wildland fire simulator. *Fire Ecol.* 20(1):71

Atchley AL, Linn R, Jonko A, Hoffman C, Hyman JD, et al. 2021. Effects of fuel spatial distribution on wildland fire behaviour. *Int. J. Wildland Fire* 30(3):179–89

Bak P, Chen K, Tang C. 1990. A forest-fire model and some thoughts on turbulence. *Phys. Lett. A* 147(5–6):297–300

Banerjee T. 2020. Impacts of forest thinning on wildland fire behavior. *Forests* 11(9):918

Banerjee T, Heilman W, Goodrick S, Hiers JK, Linn R. 2020a. Effects of canopy midstory management and fuel moisture on wildfire behavior. *Sci. Rep.* 10(1):17312

Banerjee T, Holland T, Solander K, Holmes M, Linn R. 2020b. Identifying characteristics of wildfire towers and troughs. *Atmosphere* 11(8):796

Bebieva Y, Oliveto J, Quaife B, Skowronski NS, Heilman WE, Speer K. 2020. Role of horizontal eddy diffusivity within the canopy on fire spread. *Atmosphere* 11(6):672

Bebieva Y, Speer K, White L, Smith R, Mayans G, Quaife B. 2021. Wind in a natural and artificial wildland fire fuel bed. *Fire* 4(2):30

Beer T. 1990. Percolation theory and fire spread. *Combust. Sci. Technol.* 72(4–6):297–304

Beer T. 1991. The interaction of wind and fire. *Boundary-Layer Meteorol.* 54(3):287–308

Belcher SE, Harman IN, Finnigan JJ. 2012. The wind in the willows: flows in forest canopies in complex terrain. *Annu. Rev. Fluid Mech.* 44:479–504

Bonner SR, Hoffman CM, Linn RR, Tinkham WT, Atchley AL, et al. 2024. Forest structural complexity and ignition pattern influence simulated prescribed fire effects. *Fire Ecol.* 20(1):82

Brunet Y. 2020. Turbulent flow in plant canopies: historical perspective and overview. *Boundary-Layer Meteorol.* 177(2):315–64

Buckingham E. 1914. On physically similar systems; illustrations of the use of dimensional equations. *Phys. Rev.* 4(4):345–76

Burgan RE, Rothermel RC. 1984. *BEHAVE: fire behavior prediction and fuel modeling system–FUEL subsystem*. Tech. Rep. INT-167, Forest Service, US Department of Agriculture

Byram GM. 1959. Forest fire behavior. In *Forest Fire: Control and Use*, ed. KP Davis. McGraw-Hill

Canfield J, Linn R, Sauer J, Finney M, Forthofer J. 2014. A numerical investigation of the interplay between fireline length, geometry, and rate of spread. *Agric. Forest Meteorol.* 189:48–59

Cervantes AQ, Desai A, Banerjee T. 2025. Impact of forest canopy structure on buoyant plume dynamics during wildland fires. Preprint, arXiv:2510.14423v1 [physics.flu-dyn]

Charbonneau P. 2017. *Natural Complexity: A Modeling Handbook*. Princeton University Press

Chung H, Koseff JR. 2023. Interaction of a buoyant plume with a turbulent canopy mixing layer. *Phys. Rev. Fluids* 8(6):064501

Chung H, Sunberg LK, MacDonald E, Ouellette NT, Koseff JR. 2024. Dispersion of inertial particles in turbulent canopy flows with buoyant and nonbuoyant plumes. *Phys. Rev. Fluids* 9(9):093801

Clar S, Schenk K, Schwabl F. 1997. Phase transitions in a forest-fire model. *Phys. Rev. E* 55(3):2174

Clark KL, Heilman WE, Skowronski NS, Gallagher MR, Mueller E, et al. 2020. Fire behavior, fuel consumption, and turbulence and energy exchange during prescribed fires in pitch pine forests. *Atmosphere* 11(3):242

Clark TL, Jenkins MA, Coen J, Packham DR. 1996. A coupled atmosphere-fire model: role of the convective Froude number and dynamic fingering at the fireline. *Int. J. Wildland Fire* 6(4):177–90

Clements CB, Kochanski AK, Seto D, Davis B, Camacho C, et al. 2019. The FireFlux II experiment: a model-guided field experiment to improve understanding of fire–atmosphere interactions and fire spread. *Int. J. Wildland Fire* 28(4):308–26

Clements CB, Zhong S, Goodrick S, Li J, Potter BE, et al. 2007. Observing the dynamics of wildland grass fires: FireFlux—a field validation experiment. *Bull. Am. Meteorol. Soc.* 88(9):1369–82

Coen JL, Cameron M, Michalakes J, Patton EG, Riggan PJ, Yedinak KM. 2013. WRF-Fire: coupled weather–wildland fire modeling with the weather research and forecasting model. *J. Appl. Meteorol. Climatol.* 52(1):16–38

Cunningham P, Linn RR. 2007. Numerical simulations of grass fires using a coupled atmosphere-fire model: dynamics of fire spread. *J. Geophys. Res. Atmos.* 112(D5):D05108

Curry JR, Fons WL. 1940. Forest-fire behavior studies. *Mech. Eng.* 62:219–25

Deardorff JW. 1980. Stratocumulus-capped mixed layers derived from a three-dimensional model. *Boundary-Layer Meteorol.* 18:495–527

Desai A, Cervantes AQ, Banerjee T. 2025a. Investigating buoyant plume dynamics induced by localized fire-simulated heating over plant canopies using LES. Preprint, arXiv:2510.13196v1 [physics.ao-ph]

Desai A, Cervantes AQ, Banerjee T. 2025b. Scaling analysis for buoyant plumes over wildland fires. Preprint, arXiv:2510.13189v1 [physics.ao-ph]

Desai A, Goodrick S, Banerjee T. 2022. Investigating the turbulent dynamics of small-scale surface fires. *Sci. Rep.* 12(1):10503

Desai A, Guilloteau C, Heilman WE, Charney JJ, Skowronski NS, et al. 2024. Investigating fire–atmosphere interaction in a forest canopy using wavelets. *Boundary-Layer Meteorol.* 190(5):21

Desai A, Heilman WE, Skowronski NS, Clark KL, Gallagher MR, et al. 2023. Features of turbulence during wildland fires in forested and grassland environments. *Agric. Forest Meteorol.* 338:109501

Drossel B, Schwabl F. 1992. Self-organized critical forest-fire model. *Phys. Rev. Lett.* 69(11):1629

Faraday M, Crookes W, Rossiter P. 1920. *The Chemical History of a Candle.* BiblioBytes

Finney MA. 1998. FARSITE: Fire Area Simulator–model development and evaluation. Res. Pap. RMRS-RP-4. Forest Service, US Department of Agriculture

Finney MA. 2006. An overview of FlamMap fire modeling capabilities. In *Fuels Management—How to Measure Success: Conference Proceedings*, ed. PL Andrews, BW Butler, W Bret. Forest Service, US Department of Agriculture

Finney MA, Cohen JD, Forthofer JM, McAllister SS, Gollner MJ, et al. 2015. Role of buoyant flame dynamics in wildfire spread. *PNAS* 112(32):9833–38

Finnigan J. 2000. Turbulence in plant canopies. *Annu. Rev. Fluid Mech.* 32:519–71

Finnigan JJ. 2020. The turbulent wind in plant and forest canopies. In *Plant Disturbance Ecology*. Elsevier. 2nd ed.

Fons WL. 1946. Analysis of fire spread in light forest fuels. *J. Agric. Res.* 72(3):92–121

Forthofer JM, Goodrick SL. 2011. Review of vortices in wildland fire. *J. Combust.* 2011(1):984363

Gao W, Shaw RH, Paw U KT. 1989. Observation of organized structure in turbulent flow within and above a forest canopy. *Boundary-Layer Meteorol.* 47:349–77

Graham RT, McCaffrey S, Jain TB. 2004. *Science basis for changing forest structure to modify wildfire behavior and severity.* Tech. Rep. RMRS-GTR-120, Forest Service, US Department of Agriculture

Grassberger P. 1993. On a self-organized critical forest-fire model. *J. Phys. A Math. Gen.* 26(9):2081

Grishin AM. 1996. General mathematical model for forest fires and its applications. *Combust. Explosion Shock Waves* 32(5):503–19

Harman IN, Finnigan JJ. 2007. A simple unified theory for flow in the canopy and roughness sublayer. *Boundary-Layer Meteorol.* 123:339–63

Harrington JA, Kathol E. 2009. Responses of shrub midstory and herbaceous layers to managed grazing and fire in a North American savanna (oak woodland) and prairie landscape. *Restorat. Ecol.* 17(2):234–44

Harris S, McDonald N. 2022. Fingering instability in wildfire fronts. *J. Fluid Mech.* 943:A34

Heilman WE. 2021. Atmospheric turbulence in wildland fire environments: implications for fire behavior and smoke dispersion. *Fire Manag. Today* 79(1):24–29

Heilman WE. 2023. Atmospheric turbulence and wildland fires: a review. *Int. J. Wildland Fire* 32(4):476–95

Heilman WE, Banerjee T, Clements CB, Clark KL, Zhong S, Bian X. 2021. Observations of sweep–ejection dynamics for heat and momentum fluxes during wildland fires in forested and grassland environments. *J. Appl. Meteorol. Climatol.* 60(2):185–99

Heilman WE, Clements CB, Seto D, Bian X, Clark KL, et al. 2015. Observations of fire-induced turbulence regimes during low-intensity wildland fires in forested environments: implications for smoke dispersion. *Atmos. Sci. Lett.* 16(4):453–60

Hiers JK, O'Brien JJ, Varner JM, Butler BW, Dickinson M, et al. 2020. Prescribed fire science: the case for a refined research agenda. *Fire Ecol.* 16:11

Hoff V, Rowell E, Teske C, Queen L, Wallace T. 2019. Assessing the relationship between forest structure and fire severity on the North Rim of the Grand Canyon. *Fire* 2(1):10

Hoffman CM, Linn R, Parsons R, Sieg C, Winterkamp J. 2015. Modeling spatial and temporal dynamics of wind flow and potential fire behavior following a mountain pine beetle outbreak in a lodgepole pine forest. *Agric. Forest Meteorol.* 204:79–93

Kaimal JC, Finnigan JJ. 1994. *Atmospheric Boundary Layer Flows: Their Structure and Measurement*. Oxford University Press

Karafyllidis I, Thanailakis A. 1997. A model for predicting forest fire spreading using cellular automata. *Ecol. Model.* 99(1):87–97

Katul G, Li D, Manes C. 2019. A primer on turbulence in hydrology and hydraulics: the power of dimensional analysis. *WIREs Water* 6(2):e1336

Katul GG, Cava D, Siqueira M, Poggi D. 2013. Scalar turbulence within the canopy sublayer. In *Coherent Flow Structures at Earth's Surface*, ed. JG Venditti, JL Best, M Church, RJ Hardy. Wiley

Katurji M, Noonan B, Zhang J, Valencia A, Shumacher B, et al. 2022. Atmospheric turbulent structures and fire sweeps during shrub fires and implications for flaming zone behaviour. *Int. J. Wildland Fire* 32(1):43–55

Katurji M, Zhang J, Satinsky A, McNair H, Schumacher B, et al. 2021. Turbulent thermal image velocimetry at the immediate fire and atmospheric interface. *J. Geophys. Res. Atmos.* 126(24):e2021JD035393

Kenney PM, Keith TG, Ng TT, Linn RR. 2008. In-field determination of drag through grass for a forest-fire simulation model. In *WIT Transactions on Ecology and the Environment*, Vol. 119, ed. J de las Heras, CA Brebbia, D Viegas, V Leone. WIT Press

Kiefer MT, Heilman WE, Zhong S, Charney JJ, Bian X. 2015. Mean and turbulent flow downstream of a low-intensity fire: influence of canopy and background atmospheric conditions. *J. Appl. Meteorol. Climatol.* 54(1):42–57

Kiefer MT, Heilman WE, Zhong S, Charney JJ, Bian X. 2016. A study of the influence of forest gaps on fire–atmosphere interactions. *Atmos. Chem. Phys.* 16(13):8499–509

Kiefer MT, Heilman WE, Zhong S, Charney JJ, Bian X. 2018. A numerical study of atmospheric perturbations induced by heat from a wildland fire: sensitivity to vertical canopy structure and heat source strength. *J. Geophys. Res. Atmos.* 123(5):2555–72

Kiefer MT, Zhong S, Heilman WE, Charney JJ, Bian X. 2013. Evaluation of an ARPS-based canopy flow modeling system for use in future operational smoke prediction efforts. *J. Geophys. Res. Atmos.* 118(12):6175–88

Legendre D. 2024. Fluid dynamics of airtanker firefighting. *Annu. Rev. Fluid Mech.* 56:577–603

Li S, Baijnath-Rodino JA, York RA, Quinn-Davidson LN, Banerjee T. 2025. Temporal and spatial pattern analysis of escaped prescribed fires in California from 1991 to 2020. *Fire Ecol.* 21(1):3

Linn RR, Cunningham P. 2005. Numerical simulations of grass fires using a coupled atmosphere–fire model: basic fire behavior and dependence on wind speed. *J. Geophys. Res. Atmos.* 110(D13):D13107

Linn RR, Hiers JK, O'Brien JJ, Yedinak K, Hoffman C, et al. 2025. Wildland fire entrainment: the missing link between wildland fire and its environment. *PNAS Nexus* 4(1):pgae576

Linn RR, Sieg CH, Hoffman CM, Winterkamp JL, McMillin JD. 2013. Modeling wind fields and fire propagation following bark beetle outbreaks in spatially-heterogeneous pinyon-juniper woodland fuel complexes. *Agric. Forest Meteorol.* 173:139–53

Linn RR, Winterkamp J, Colman JJ, Edminster C, Bailey JD. 2005. Modeling interactions between fire and atmosphere in discrete element fuel beds. *Int. J. Wildland Fire* 14(1):37–48

Loudermilk EL, O'Brien JJ, Goodrick SL, Linn RR, Skowronski NS, Hiers JK. 2022. Vegetation's influence on fire behavior goes beyond just being fuel. *Fire Ecol.* 18(1):9

Mallia DV, Kochanski AK, Urbanski SP, Mandel J, Farguell A, Krueger SK. 2020. Incorporating a canopy parameterization within a coupled fire-atmosphere model to improve a smoke simulation for a prescribed burn. *Atmosphere* 11(8):832

Mandel J, Beezley JD, Kochanski AK. 2011. Coupled atmosphere-wildland fire modeling with WRF-Fire version 3.3. *Geosci. Model Dev. Discuss.* 4(1):497–545

Marcozzi A, Wells L, Parsons R, Mueller E, Linn R, Hiers JK. 2025. FastFuels: advancing wildland fire modeling with high-resolution 3D fuel data and data assimilation. *Environ. Model. Softw.* 183:106214

McKenzie D, Miller C, Falk DA, eds. 2011. *The Landscape Ecology of Fire*. Springer Science & Business Media

Mercer GN, Weber RO. 1994. Plumes above line fires in a cross-wind. *Int. J. Wildland Fire* 4(4):201–7

Michaletz ST, Johnson EA. 2006. A heat transfer model of crown scorch in forest fires. *Can. J. Forest Res.* 36(11):2839–51
Moinuddin KAM, Sutherland D. 2020. Modelling of tree fires and fires transitioning from the forest floor to the canopy with a physics-based model. *Math. Comput. Simul.* 175:81–95
Morvan D. 2011. Physical phenomena and length scales governing the behaviour of wildfires: a case for physical modelling. *Fire Technol.* 47(2):437–60
Morvan D, Frangieh N. 2018. Wildland fires behaviour: wind effect versus Byram's convective number and consequences upon the regime of propagation. *Int. J. Wildland Fire* 27(9):636–41
Mueller E, Mell W, Simeoni A. 2014. Large eddy simulation of forest canopy flow for wildland fire modeling. *Can. J. Forest Res.* 44(12):1534–44
Mueller EV, Gallagher MR, Skowronski N, Hadden RM. 2021a. Approaches to modeling bed drag in pine forest litter for wildland fire applications. *Transport Porous Media* 136:637–60
Mueller EV, Skowronski NS, Clark KL, Gallagher MR, Mell WE, et al. 2021b. Detailed physical modeling of wildland fire dynamics at field scale—an experimentally informed evaluation. *Fire Saf. J.* 120:103051
Nelson RM. 1993. Byram derivation of the energy criterion for forest and wildland fires. *Int. J. Wildland Fire* 3(3):131–38
Nepf HM. 2012. Flow and transport in regions with aquatic vegetation. *Annu. Rev. Fluid Mech.* 44:123–42
Ohtsuki T, Keyes T. 1986. Biased percolation: forest fires with wind. *J. Phys. A Math. Gen.* 19(5):L281
Pagni PJ, Peterson TG. 1973. Flame spread through porous fuels. *Symp. (Int.) Combust.* 14(1):1099–107
Patton EG, Finnigan JJ. 2012. Canopy turbulence. In *Handbook of Environmental Fluid Dynamics*, Vol. 1, ed. HJ Fernanco. CRC Press
Paw U KT, Snyder RL, Spano D, Su HB. 2005. Surface renewal estimates of scalar exchange. *Micrometeorol. Agric. Syst.* 47:455–83
Petersen AJ, Banerjee T. 2024. Characterizing firebrands and their kinematics during lofting. *Phys. Fluids* 36(10):106611
Peterson DL, Johnson MC, Agee JK, Jane TB, McKenzie D, Reinhardt ED. 2005. *Forest structure and fire hazard in dry forests of the Western United States.* Tech. Rep. PNW-GTR-628, Forest Service, US Department of Agriculture
Pimont F, Dupuy J-L, Linn RR, Dupont S. 2011. Impacts of tree canopy structure on wind flows and fire propagation simulated with FIRETEC. *Ann. Forest Sci.* 68(3):523–30
Poggi D, Porporato A, Ridolfi L, Albertson J, Katul G. 2004. The effect of vegetation density on canopy sub-layer turbulence. *Boundary-Layer Meteorol.* 111:565–87
Raupach MR, Thom AS. 1981. Turbulence in and above plant canopies. *Annu. Rev. Fluid Mech.* 13:97–129
Raupach MR. 1990. Similarity analysis of the interaction of bushfire plumes with ambient winds. *Math. Comput. Model.* 13(12):113–21
Raymond CL, Peterson DL. 2005. Fuel treatments alter the effects of wildfire in a mixed-evergreen forest, Oregon, USA. *Can. J. Forest Res.* 35(12):2981–95
Rothermel RC. 1972. A mathematical model for predicting fire spread in wildland fuels. Res. Pap. INT-115, Forest Service, US Department of Agriculture
Rothermel RC. 1991. Predicting behavior and size of crown fires in the northern Rocky Mountains. Res. Pap. INT-438, Forest Service, US Department of Agriculture
Rui X, Hui S, Yu X, Zhang G, Wu B. 2018. Forest fire spread simulation algorithm based on cellular automata. *Natural Hazards* 91:309–19
Safford HD, Schmidt DA, Carlson CH. 2009. Effects of fuel treatments on fire severity in an area of wildland–urban interface, Angora Fire, Lake Tahoe Basin, California. *Forest Ecol. Manag.* 258(5):773–87
Shaw RH, Schumann U. 1992. Large-eddy simulation of turbulent flow above and within a forest. *Boundary-Layer Meteorol.* 61(1):47–64
Shaw RH, Silversides RH, Thurtell GW. 1974. Some observations of turbulence and turbulent transport within and above plant canopies. *Boundary-Layer Meteorol.* 5:429–49
Show SB. 1919. Climate and forest fires in northern California. *J. Forestry* 17(8):965–79
Stephens SL, Moghaddas JJ, Edminster C, Fiedler CE, Haase S, et al. 2009. Fire treatment effects on vegetation structure, fuels, and potential fire severity in western U.S. forests. *Ecol. Appl.* 19(2):305–20

Sullivan AL. 2007. Convective Froude number and Byram's energy criterion of Australian experimental grassland fires. *Proc. Combust. Inst.* 31(2):2557–64

Sullivan AL. 2017. Inside the inferno: fundamental processes of wildland fire behaviour. *Curr. Forestry Rep.* 3(2):150–71

Thomas PH. 1963. The size of flames from natural fires. *Symp. (Int.) Combust.* 9(1):844–59

Tieszen SR. 2001. On the fluid mechanics of fires. *Annu. Rev. Fluid Mech.* 33:67–92

Tohidi A, Gollner MJ, Xiao H. 2018. Fire whirls. *Annu. Rev. Fluid Mech.* 50:187–213

Valencia A, Melnik KO, Sanders N, Hoy AS, Yan M, et al. 2023. Influence of fuel structure on gorse fire behaviour. *Int. J. Wildland Fire* 32(6):927–41

Van Wagner CV. 1977. Conditions for the start and spread of crown fire. *Can. J. Forest Res.* 7(1):23–34

Wright J. 1932. *Forest-fire hazard research as developed and conducted at the Petawawa Forest Experiment Station.* Inf. Rep. FF-X-5, Forest Fire Research Institute

Zhang K, Lamorlette A. 2020. An extensive numerical study of the burning dynamics of wildland fuel using proposed configuration space. *Int. J. Heat Mass Transf.* 160:120174

Zhang K, Verma S, Trouvé A, Lamorlette A. 2020. A study of the canopy effect on fire regime transition using an objectively defined Byram convective number. *Fire Saf. J.* 112:102950